Quaternary Research 83 (2015) 80–93

Contents lists available at ScienceDirect

Quaternary Research

journal homepage: www.elsevier.com/locate/yqres

# Constraints on paleoclimate from 11.5 to 5.0 ka from shoreline dating and hydrologic budget modeling of Baqan Tso, southwestern Tibetan Plateau

Tyler Huth [a,*], Adam M. Hudson [b], Jay Quade [b], Lei Guoliang [c], Zhang Hucai [d]

[a] Department of Geology and Geophysics, University of Utah, Salt Lake City, UT, USA
[b] Department of Geosciences, University of Arizona, Tucson, AZ 85721, USA
[c] College of Geographical Sciences, Fujian Normal University, Fujian 350007, China
[d] College of Tourism and Geography, Yunnan Normal University, Kunming 650500, China

ARTICLE INFO

*Article history:*
Received 25 March 2014
Available online 22 September 2014

*Keywords:*
Tibetan Plateau
Paleolake
Carbon-14 dating
Holocene
Shoreline dating
Paleohydrologic model
Precipitation
Monsoon

ABSTRACT

$^{14}$C dating of shoreline deposits of closed-basin lake Baqan Tso in the western Tibetan Plateau shows that lake level regressed from the undated highstand (46 m above modern, 4.3× modern surface area) of likely earliest Holocene age by 11.5 ka, and remained larger than modern until at least ≈5.0 ka. The shoreline record broadly matches other regional climate records, with lake level closely following Northern Hemisphere summer insolation overprinted by sub-millennial lake-level oscillations. A model coupling modern land runoff and lake surface heat closely reproduces estimated modern precipitation of ≈240 mm/yr. We estimate that the Baqan Tso basin required ≈380 mm/yr precipitation to sustain the maximum early Holocene lake area, a 55% increase over modern. Precipitation increases, not glacial meltwater, drove lake-level changes, as Baqan Tso basin was not glaciated during the Holocene. Our estimate assumes early Holocene insolation (≈1.3% overall increase), and mean annual increases of 2°C in temperature, and 37% in relative humidity. We additionally developed a Holocene precipitation history for Baqan Tso using dated paleolake areas. Using the modern and early Holocene model results as end-members, we estimate precipitation in the western Tibetan Plateau which was 300–380 mm/yr between 5.0 and 11.5 ka, with error of ±29–57 mm/yr (±12–15%).



## Introduction

Asian Summer Monsoon precipitation provides water resources to over half of the Earth's population. Therefore it is important to understand past variations in the monsoon's strength and duration during past warmer global climate when attempting to make projections about how it will vary in response to future climate change. Much of Asia is expected to warm during the next century, but climate models inadequately represent the Tibetan Plateau and disagree on projections of future precipitation change. Some of the difficulty with accurately predicting future rainfall response is due to few instrumental observations and a limited distribution of paleoclimate records (Christensen et al., 2007). Available instrumental and paleoclimate records indicate a centennial- to millennial-scale link between Asian Monsoon strength and North Atlantic climate, ENSO, Eurasian snow cover, aerosols, and vegetation changes (Christensen et al., 2007). On long timescales, speleothem $\delta^{18}$O records suggest that monsoon precipitation amount is forced by orbital cyclicity of Northern Hemisphere summer insolation (e.g. Wang et al., 2008). Solar forcing may also modulate millennial-scale changes in monsoon strength (Gupta et al., 2003; 2005). The response to these controls in the timing and probable magnitude of monsoonal rainfall varies across the monsoon region (An et al., 2000).

For the Tibetan Plateau, many monsoon paleoclimate records rely on core-based proxy evidence from lakes to estimate changes in monsoon rainfall amount (e.g., Demske et al., 2009; Gasse et al., 1996; Herzschuh et al., 2006b; Li et al., 2011; Lu et al., 2011; Mischke et al., 2008; Morrill et al., 2006; Mügler et al., 2010; Shen et al., 2005; Van Campo and Gasse, 1993; Wischnewski et al., 2011). However, most proxy records provide at best a semi-quantitative estimate of past variations in rainfall amount. In this study, we use shoreline deposits from paleolakes to reconstruct a quantitative history of changes in paleorainfall. Shoreline deposits do not provide continuous high-resolution climate records, but do provide a quantitative record of large hydrologic changes to the lake system through the relationship between the basin water budget and the exact surface areas for the paleolake system at shoreline levels of known age. In closed-basin lakes, the ratio of lake surface area to total drainage basin area is directly controlled by this hydrologic budget (Benson and Paillett, 1989; Hudson and Quade, 2013). Because this relationship can be estimated numerically with hydrologic modeling, shoreline deposits are an ideal method for quantifying past hydrologic changes of paleolakes down to millennial time-scales.

Baqan Tso, the focus of this study, is a closed-basin lake located in a currently nonglaciated basin with no evidence for previous glaciation (Figs. 1 and 2). This makes the system ideal for modeling paleohydrology,

* Corresponding author.
*E-mail address:* tyler.huth@utah.edu (T. Huth).

http://dx.doi.org/10.1016/j.yqres.2014.07.011
0033-5894/

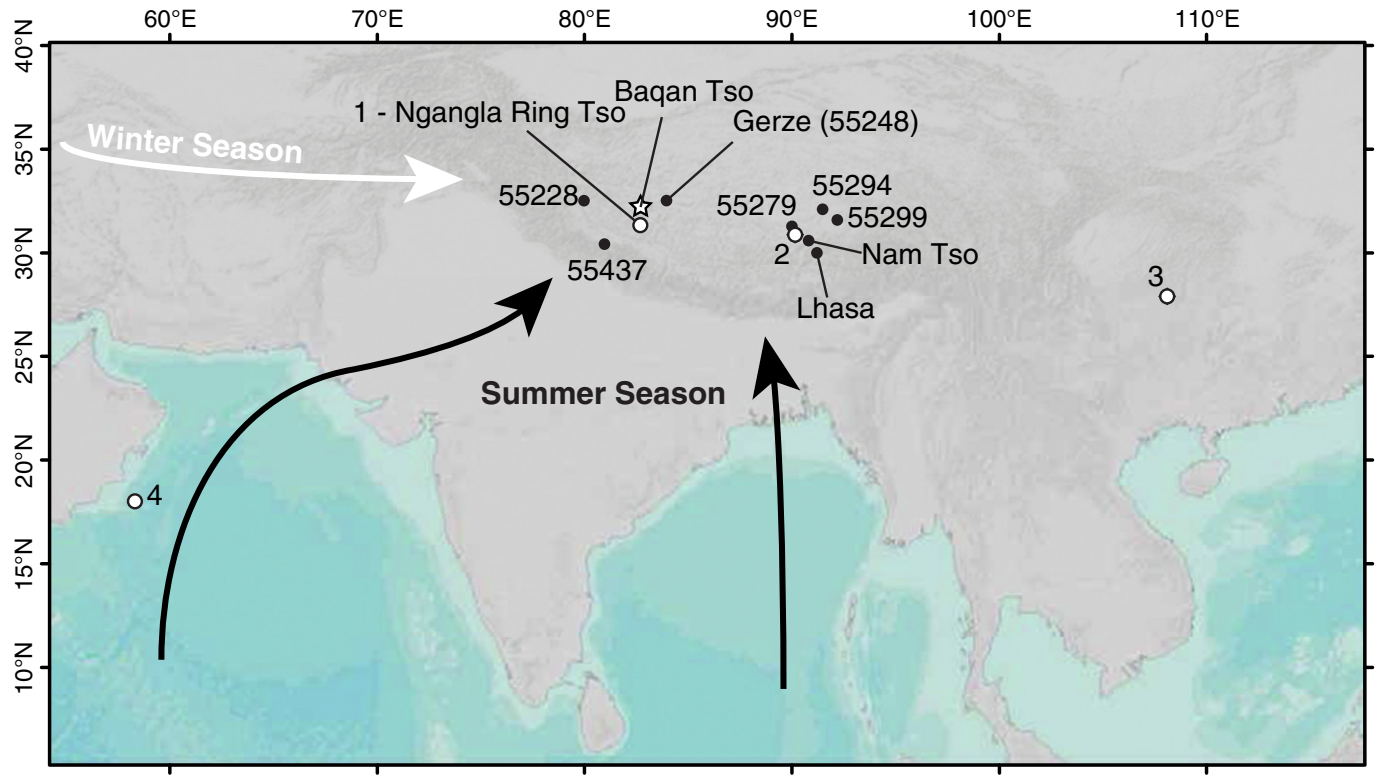


**Figure 1.** Indian Monsoon Region Overview. Study area location is shown by open star. Schematic paths of summer (gray) and winter (white) precipitation onto the western Tibetan Plateau are shown by the bold arrows. Modern weather stations and Nam Tso (Haginoya et al., 2009), used for estimating Baqan Tso climate, are designated by filled circles and associated numbers. Paleoclimate records for comparison in Fig. 7 are designated by open circles. Lhasa and the Baqan Tso region are ≈800 km apart. References are: 1 — Ngangla Ring Tso, Hudson et al., 2014-in this issue; 2 — Tianmen Cave, Cai et al., 2012; 3 — Dongge Cave, Wang et al., 2005; 4 — ODP 723, Gupta et al., 2003.

because it eliminates the demonstrated complexity that glacial melt runoff adds to lake hydrologic budgets on the Tibetan Plateau (Hudson and Quade, 2013). Collaborative work at nearby Ngangla Ring Tso (NRT; Fig. 1) has produced a more detailed history of lake-level changes for the entire Holocene (Hudson et al., 2014-in this issue) (Fig. 7). However, the NRT catchment is large, complex, and glaciated, and thus is less suitable for hydrologic modeling. We present here a new companion shoreline chronology to the NRT record and a hydrologic model that quantifies

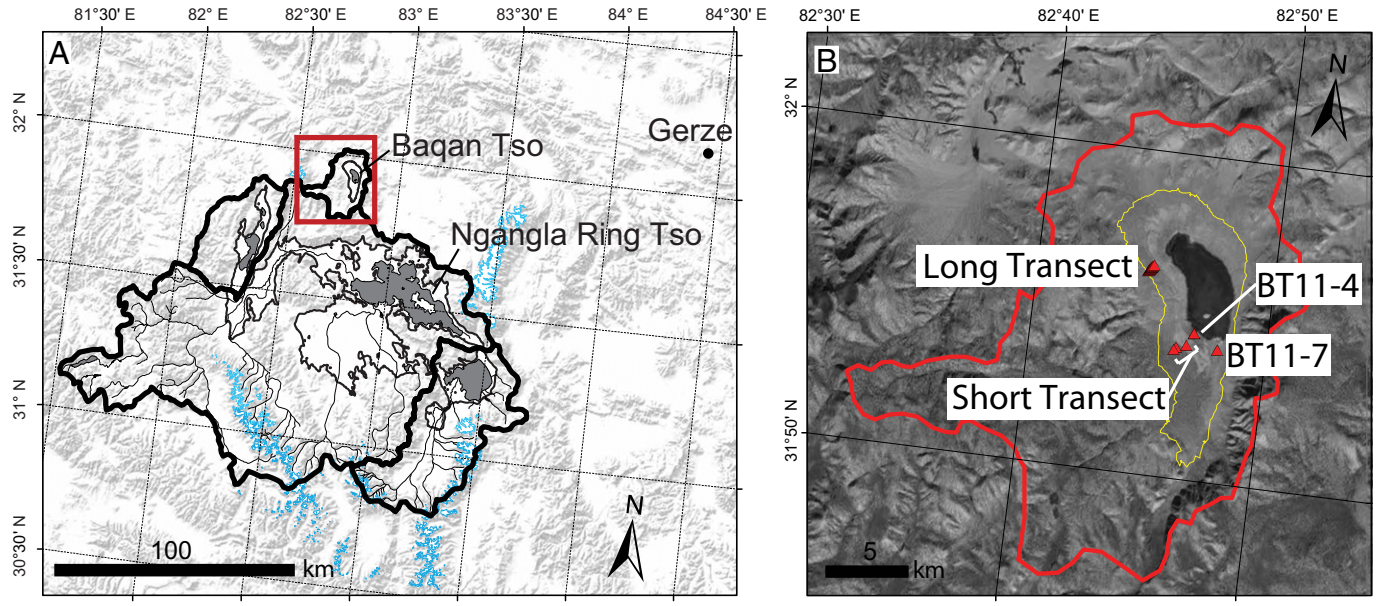


**Figure 2.** (A) The Baqan Tso region showing modern lake extents (gray), maximum early Holocene highstands (thin line), the hydrographic basins (thick line), and perennial river systems (trace lines). Red box around Baqan Tso denotes view shown in (B). (B) Landsat image of Baqan Tso showing the hydrographic basin outline (thick line), locations of sample sites (filled triangles), two sampling transects, and maximum early Holocene paleoshoreline at 5043 m (thin line). Overlapping triangles in the Long Transect represent ten distinct locations.

https://doi.org/10.1016/j.yqres.2014.07.011 Published online by Cambridge University Press

the paleoclimate changes for western Tibet required to produce the observed Holocene paleolake areas at Baqan Tso.

### *Physical setting and lacustrine deposits*

The Baqan Tso basin is located in the southwestern Tibetan Plateau (31°55.82′N 82°47.01′E). The drainage basin, covering 376 km$^2$, is a half-graben bounded by a north–south trending normal fault on the eastern side (Fig. 2). We cannot rule out any Holocene tectonic activity, but we have no evidence that such activity could have substantially altered basin drainage or lake level and complicated the climate record developed here. The bedrock within the basin is composed mostly of Tertiary volcanic rocks with no apparent carbonate (Styron et al., 2013). The basin is fed by a few small modern streams (Fig. 2) and has remained hydrographically closed at all shoreline levels. The modern lake area, derived from 1998 to 2010 sequential Landsat imagery, averages 14 km$^2$, or about 3.7% of the total basin area, at a shoreline elevation of 4977 m asl.

Well-defined shoreline benches visible along the slopes of the basin clearly define larger past lake extents. The benches form continuous rings around the basin that range in elevation from 5023 m asl (46 m above modern) to the modern lake elevation and in area up to 4.3 times the modern lake. Geomorphically, each bench is characterized by a boulder and gravel crest with a sharp slope change at the shoreward edge of the bench. Fine, light-colored sediments are located on the landward, or back-bar, side of shoreline crests but are noticeably absent on slopes between benches, producing a striped light/dark map pattern.

Lacustrine carbonate, used for $^{14}$C dating in this study, is common in these back-bar deposits as clasts of dense, sometimes layered, lithoid tufa, and as fine calcareous sediment (marl) (Fig. 3). Fossil shell is conspicuously absent. The lithoid tufa clasts are generally tabular, subrounded to angular, and 1–4 cm in diameter. The layering evident in some of this tufa likely accreted during repeated lake transgressions and regressions. The tufa clasts are largely unreworked or disturbed since deposition, judging from their angularity and the pristine, uneroded appearance of the shorelines themselves. The probable modern analog environment for lithoid-tufa formation is visible along the margin of Baqan Tso today, where we observed highly evaporated back-bar pools containing a mix of fine grained calcareous sediment and dispersed sand and gravel. Lithoid tufa clasts exhibiting mud cracks are preserved near the modern shoreline and in soil pit BT11-19 (Fig. 3A).

### *Regional climate*

The Indian Summer Monsoon dominates modern precipitation in southwestern Tibet (Conroy and Overpeck, 2011). Modern precipitation, based on the monthly Tropical Rainfall Measuring Mission (TRMM) data from 1998 to 2009, is ≈240 mm/yr for the grid cell containing the Baqan Tso basin (Kummerow et al., 1998). Approximately 60–80% of precipitation falls during the summer, mostly between May and October (Tian et al., 2007; Bookhagen, 2010). Seasonal average temperatures at the nearby (150 km away) Gerze weather station (station 55248) range from −11°C in the winter to 10°C in the summer, with an annual average just above freezing (Li et al., 2010) (Fig. 2A). Precipitation at Gerze has the same seasonality as at Baqan Tso (Conroy and Overpeck, 2011). However, precipitation is slightly less than that for Baqan Tso because the Gerze weather station (≈4425 m asl) is ≈550 m lower than Baqan Tso (4977 m asl) and lies further inland. An assumed lapse rate of 7°C/km would give temperatures approximately 3°C colder at Baqan Tso, with a winter average of −14°C, a summer average of 7°C, and an annual average of −3°C (Fig. 4).

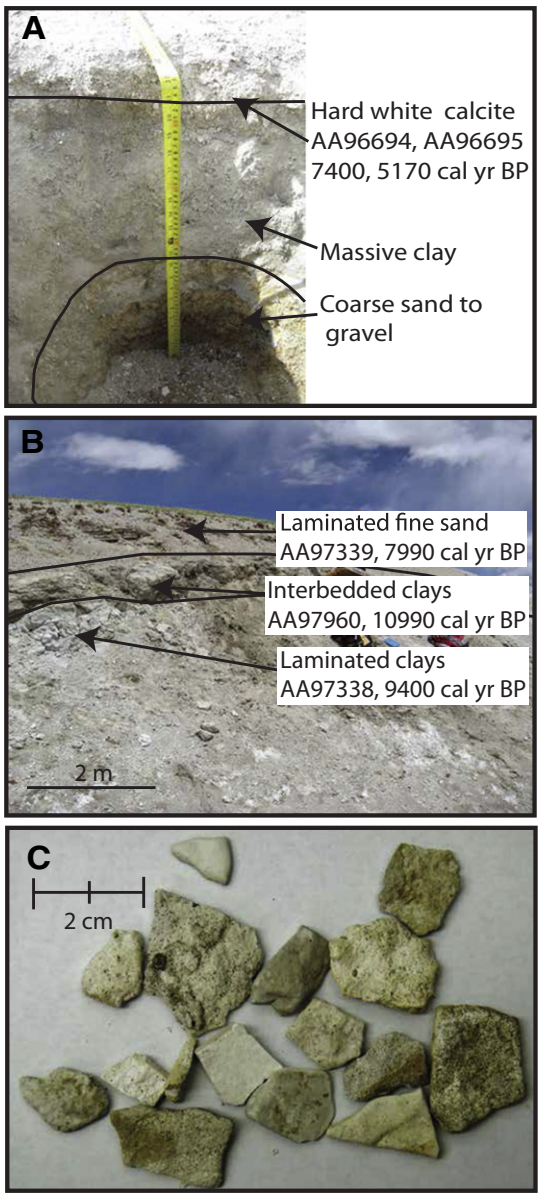


**Figure 3.** (A) Exposure at BT11-19; pit is 55 cm deep. See Fig. 6C for description. (B) Exposure at BT11-7; measured section is 190 cm. See Fig. 6A for description. (C) Representative lithoid-tufa clasts used in $^{14}$C dating sampled from a Baqan Tso paleolake shoreline.

## Methods

### *Sample collection*

Locations and elevations of sampling sites were measured using a high-precision Trimble GeoXH GPS unit. Modern aquatic plant material was collected living from the lake shoreline. Most geologic samples were collected along two transects that extend through the paleoshorelines. The Long Transect extends westward from Baqan Tso, covering all sampled paleoshorelines, and the Short Transect extends southward of the lake, covering only the shallower paleoshorelines up to 5001 m asl (Fig. 2B). Lithoid tufa for $^{14}$C dating was collected from the shoreward termination of each bench along these transects. Along the Long Transect west of the lake, we also described and sampled stratigraphic sections in ≈1 m-deep hand trenches dug in shoreline or back-bar sediments (Fig. 2B). At site BT11-7 (Fig. 2B), we collected lithoid tufa and carbonate lake sediment samples from measured depths in a stratigraphic section, utilizing a natural exposure. Lithoid tufa clasts are

https://doi.org/10.1016/j.yqres.2014.07.011 Published online by Cambridge University Press

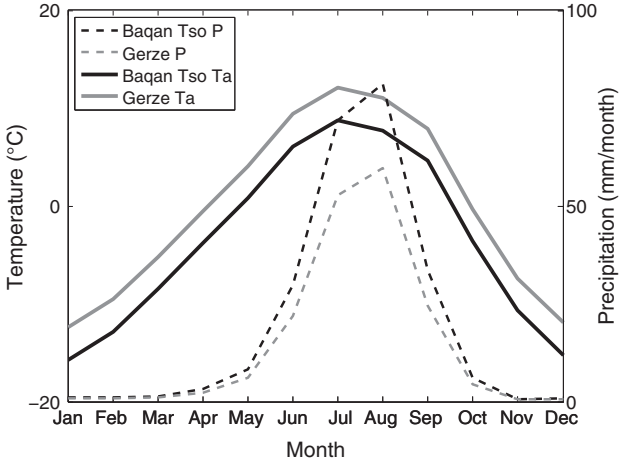


**Figure 4.** Gerze meteorological station (see Fig. 1 for location) climatologic data for western Tibetan Plateau. Monthly averaged temperature and precipitation for the period 1973–2006 are shown in gray solid and dashed lines, respectively. Baqan Tso temperature (MAT-3.9°C) and precipitation (1.40*MAP) corrected monthly averaged temperature and precipitation for the period 1973–2006 are shown in black solid and dashed lines, respectively.

absent on the highest three shorelines, including the highstand at 5023 m asl (46 m above the 2011 lake). The highest paleolake shoreline with dateable tufa is at 5014 m asl.

*Radiocarbon dating*

All sample preparation was performed at an in-house $^{14}C$ laboratory at University of Arizona. We obtained single $^{14}C$ dates from most lithoid tufa clasts. Dates from the uppermost and lowermost layers were obtained from samples that showed well-developed layering, although upper and lower are arbitrary designations because the original clast orientation is uncertain. Lithoid tufa clasts and calcareous sediment were cleaned ultrasonically, soaked in 3% $H_2O_2$, and rinsed thoroughly in distilled water. 1–2 mm pieces of intact tufa were reacted with 100% $H_3PO_4$ under vacuum until fully dissolved. Modern aquatic plant material was prepared using a standard acid–base-acid treatment and combusted under vacuum in the presence of Ag and CuO at 900°C. All sample gases were extracted under vacuum, cryogenically purified and passed through a 600°C Cu/Ag furnace to remove contaminants. Purified $CO_2$ samples were graphitized using 100 mg of zinc powder and Fe powder in a 2:1 proportion to the mass of carbon in the sample. AMS and $\delta^{13}C$ measurements were performed by the Arizona AMS Laboratory. Radiocarbon ages ($^{14}C$ yr BP) were calibrated using the CALIB 6.0 software with the IntCal09 calibration curve (Reimer et al., 2009; Stuiver and Reimer, 1993) (Table 1).

## Results

We obtained a total of 29 radiocarbon dates on aquatic plant material, lithoid tufa, pedogenic carbonate, and marl from the modern and paleoshoreline surfaces and in situ in stratigraphic sections. Our results range in age from post-bomb to 9640 ± 30 $^{14}C$ yr BP (Table 1). Modern aquatic plant material was dated to test the $^{14}C$ reservoir effect for the lake system. Tufa dates combined with sedimentologic observations define the Holocene lake level chronology.

*Reservoir effect considerations*

Lakes on the Tibetan Plateau commonly show reservoir effects of 1000–3000 yr, but up to ≈20,000 yr (Hou et al., 2012; Mischke et al., 2013). In addition, reservoir effects are known to vary through time and by site location within a lake due to changes in water source and lake level (Mischke et al., 2013). Previous researchers have used several methods in calculating the reservoir effect: determining a single point correction from a modern sample (Doberschütz et al., 2014), comparing terrestrial plant age to bulk $^{14}C$ age (Mischke et al., 2008), using an age-depth linear extrapolation to the sediment surface (Mügler et al., 2010), and comparing $^{14}C$ ages to independently derived ages (Kasper et al., 2012; Hudson et al., 2014-in this issue).

We use a single point correction, consider physical characteristics of Baqan Tso, and compare our record with that of nearby, $^{14}C$–U/Th dated Ngangla Ring Tso in determining the reservoir effect at Baqan Tso. Modern aquatic plants growing in Baqan Tso yielded a post-bomb age, 1.04 times the ratio in pre-nuclear atmosphere. This is close to the current value of atmospheric $CO_2$ (Levin et al., 2013) and suggests that the modern $^{14}C$ reservoir effect in Baqan Tso is minimal. We did not obtain actively forming lithoid tufa from the modern lake to assess the reservoir effect in this material, but physical and climatologic characteristics of Baqan Tso support $^{14}C$ equilibration with atmospheric $CO_2$ for all lake shorelines. Modern rainfall rates for the lake basin are ≈240 mm/yr (Kummerow et al., 1998). Assuming modest lake evaporation rates of 600–800 mm/yr (Haginoya et al., 2009), even the highstand lake (≈40 m deep) has only a ≈100 yr residence time. Seasonal freezing for 4–5 months per year makes long-term stratification unlikely. We did not observe paleosprings along either sample transect, with the two known spring deposits in the southern part of the basin and along the western edge of the lake, away from sampled locations. The absence of carbonate bedrock in the drainage basin also indicates little $^{14}C$-deficient carbon contributed to the dissolved carbon budget. The authors of the nearby Ngangla Ring Tso record assessed reservoir effects in time and space by comparing ages from carbonate at multiple locations at a single elevation and paired $^{14}C$–U/Th dates within single samples. Radiocarbon and U/Th dates on lacustrine carbonate at Ngangla Ring Tso agree (with a ≈165 yr reservoir effect) where sample material is located far from spring sources and the overall proportion of spring water to river discharge to the lake is small (Hudson et al., 2014-in this issue) The similarity of the Baqan Tso lake-shoreline record to the Ngangla Ring Tso record (Fig. 7) suggests a negligible reservoir effect through time. Using a single-point correction is appropriate for a Baqan Tso, as it has minimal external $^{14}C$-deficient carbon and a comparable, more extensively dated lake nearby with a small reservoir effect. Thus, we report all $^{14}C$ dates defining the lake level chronology with no reservoir-age correction.

*Lithoid tufa shoreline ages*

A total of eighteen individual $^{14}C$ dates on lithoid tufa from nine separate shoreline localities define the lake level curve for Baqan Tso (Table 1; Fig. 5). These ages range from 4510 ± 30 to 9620 ± 30 $^{14}C$ yr BP. Each age, or pair of ages where top and bottom layers were evident, comes from an individual tufa clast formed in the back-bar environment associated with a particular shoreline bench. Sampling sites BT11-12 to -19 are located in the Long Transect west of the lake. Sampling sites BT11-20 to -22 are located in the Short Transect south of the lake (Fig. 2). Replicate dates were produced for multiple tufa clasts from sites BT11-15 and 22. Ages on multiple clasts from BT11-15 range across 1350 $^{14}C$ yr and ages for clasts from BT11-22 range across 1500 $^{14}C$ yr (Table 1; Fig. 5).

*Stratigraphy and depositional sequence*

Three natural and artificial exposures of lake sediments reveal the basic shoreline stratigraphy, the associations with carbonate clasts used for dating, and temporal patterns of lake transgression and regression (Fig. 6).

https://doi.org/10.1016/j.yqres.2014.07.011 Published online by Cambridge University Press

**Table 1**
$^{14}$C results from Baqan Tso.

| Sample # | AMS# | Sample material | Elevation above lake (m)[a] | Elevation asl (m) | $\delta^{13}$C (PDB) | Fmc[b] | $^{14}$C age (yr BP) | 2-Sigma calibrated range (cal yr BP) | Median age (cal yr BP)[c] |
|---|---|---|---|---|---|---|---|---|---|
| BT11-4A | AA97959 | Modern aquatic plants | 0 | 4977 | 26.2 | 1.0406 ± 0.0001 | Post-bomb | Modern | – |
| BT11-7 0–5 cm | AA97338 | Marl | 1 | 4978 | 4.4 | 0.3519 ± 0.0010 | 8390 ± 20 | 9320–9480 | 9400 |
| BT11-7 80–90 cm | AA97960 | Marl | 1 | 4978 | 2.9 | 0.3010 ± 0.0011 | 9640 ± 30 | 10,790–11,180 | 10,990 |
| BT11-7 130–135 cm | AA97339 | Marl | 1 | 4978 | 2.8 | 0.4097 ± 0.0010 | 7170 ± 20 | 7950–8020 | 7990 |
| BT11-12 Bottom | AA97430 | Lithoid tufa | 37 | 5014 | 3.0 | 0.3434 ± 0.0010 | 8590 ± 20 | 9530–9550 | 9540 |
| BT11-12 Top | AA97429 | Lithoid tufa | 37 | 5014 | 2.6 | 0.3018 ± 0.0011 | 9620 ± 30 | 10,790–11,170 | 10,980 |
| BT11-13 A | AA97340 | Lithoid tufa | 32 | 5009 | 5.5 | 0.3507 ± 0.0010 | 8420 ± 20 | 9430–9490 | 9460 |
| BT11-13 B | AA97341 | Lithoid tufa | 32 | 5009 | 5.7 | 0.4056 ± 0.0010 | 7250 ± 20 | 8010–8160 | 8080 |
| BT11-13B rep 1 | AA98619 | Lithoid tufa | 32 | 5009 | 4.3 | 0.3360 ± 0.0019 | 8760 ± 50 | 9560–9920 | 9740 |
| BT11-13B rep 2 | AA98625 | Lithoid tufa | 32 | 5009 | 4.8 | 0.3621 ± 0.0020 | 8160 ± 40 | 9010–9260 | 9130 |
| BT11-13 C | AA97342 | Pedogenic carbonate | 32 | 5009 | −2.1 | 0.7281 ± 0.0004 | 2550 ± 30 | 2500–2750 | 2620 |
| BT11-14 A | AA97343 | Lithoid tufa | 29 | 5006 | 4.9 | 0.4055 ± 0.0010 | 7250 ± 20 | 8010–8160 | 8080 |
| BT11-15 A | AA97345 | Lithoid tufa | 27 | 5004 | 5.5 | 0.3589 ± 0.0010 | 8230 ± 20 | 9120–9290 | 9210 |
| BT11-15A rep 1 | AA98626 | Lithoid tufa | 27 | 5004 | 3.4 | 0.4012 ± 0.0019 | 7340 ± 40 | 8020–8300 | 8160 |
| BT11-15A rep 2 | AA98621 | Lithoid tufa | 27 | 5004 | 5.0 | 0.4353 ± 0.0020 | 6680 ± 40 | 7480–7610 | 7550 |
| BT11-16 A | AA97347 | Lithoid tufa | 26 | 5003 | 4.6 | 0.3736 ± 0.0010 | 7910 ± 20 | 8610–8950 | 8780 |
| BT11-17 A Bottom | AA97432 | Lithoid tufa | 26 | 5003 | 3.0 | 0.3981 ± 0.0010 | 7400 ± 20 | 8180–8310 | 8240 |
| BT11-17 A Top | AA97431 | Lithoid tufa | 26 | 5003 | 1.2 | 0.3683 ± 0.0010 | 8020 ± 20 | 8780–9010 | 8890 |
| BT11-18A Bottom | AA96389 | Lithoid tufa | 23 | 5000 | 6.3 | 0.4479 ± 0.0021 | 6450 ± 40 | 7290–7430 | 7360 |
| BT11-18A Top | AA96388 | Lithoid tufa | 23 | 5000 | 5.0 | 0.4917 ± 0.0022 | 5700 ± 40 | 6400–6630 | 6520 |
| BT11-19A Bottom | AA96695 | Lithoid tufa | 21 | 4998 | 5.8 | 0.4440 ± 0.0020 | 6520 ± 40 | 7330–7550 | 7440 |
| BT11-19A Top | AA96694 | Lithoid tufa | 21 | 4998 | 6.6 | 0.5703 ± 0.0022 | 4510 ± 30 | 5050–5300 | 5170 |
| BT11-20A Bottom | AA96697 | Lithoid tufa | 16 | 4993 | 7.5 | 0.5442 ± 0.0020 | 5180 ± 10 | 5910–5940 | 5930 |
| BT11-20A Top | AA96696 | Lithoid tufa | 16 | 4993 | 6.8 | 0.4910 ± 0.0020 | 5710 ± 30 | 6410–6570 | 6490 |
| BT11-21A Bottom | AA96391 | Lithoid tufa | 20 | 4997 | 4.9 | 0.4626 ± 0.0021 | 6190 ± 40 | 6970–7240 | 7110 |
| BT11-21A Top | AA96390 | Lithoid tufa | 20 | 4997 | 5.6 | 0.4700 ± 0.0022 | 6060 ± 40 | 6790–7010 | 6900 |
| BT11-22 A | AA97350 | Lithoid tufa | 24 | 5001 | 4.7 | 0.3228 ± 0.0011 | 9080 ± 30 | 10,200–10,260 | 10,230 |
| BT11-22A rep 1 | AA98622 | Lithoid tufa | 24 | 5001 | 4.7 | 0.3642 ± 0.0019 | 8110 ± 40 | 8980–9140 | 9060 |
| BT11-22A rep 2 | AA98623 | Lithoid tufa | 24 | 5001 | 4.1 | 0.3894 ± 0.0019 | 7580 ± 40 | 8340–8440 | 8390 |

[a] Elevation above lake (m) — meters above present day Bachan Tso.
[b] Fmc is fraction modern carbon and includes lab blank correction (specific to each run, or running average).
[c] Calibrated with CALIB 6.0 — Intcal 09, years BP (before present–AD 1950) at 2σ, or full range if 2σ estimate not made at 95% confidence.

*BT11-7 (4978 m asl, 1 m above modern lake)*

Section BT11-7 is located in an exposure of lake sediments along the bank of the main stream channel feeding Baqan Tso from the south. The sequence exposed in BT11-7 likely formed during lake regression. The bottom of BT11-7 exposes highly calcareous laminated clay consistent with deep water deposition (0–90 cm; Fig. 3, Fig. 6). Dates from marl at the base and top of this layer are inverted, yielding ages of 9320–9480 (AA97338) and 10790–11180 (AA97960) cal yr BP, respectively. The laminated clay grades upwards into alternating hard iron-stained and whiter, slightly hard clay layers (90–135 cm), representing a shallower environment with one marl dating to 7950–8020 cal yr BP (AA97339). The upper section is highly calcareous, laminated fine sand with gently undulating bedding deposited in a distal deltaic environment (135–189 cm). The sequence is capped by a thin organic-rich horizon (189–190 cm) resulting from post-lake pedogenesis.

*BT11-13 (5009 m asl, 32 m above modern lake)*

A soil pit dug at BT11-13 is the higher of two pits dug in the Long Transect of paleoshorelines to the west of the lake (Fig. 2). The sequence exposed in BT11-13 likely formed during a lake regression ending by 9.5 ka (Fig. 6). The lowermost portion of the sequence (0–15 cm) is composed of weakly bedded, moderately calcareous sand with dispersed pebbles, consistent with a near shore beach environment (Fig. 6). This sequence grades upward into interbedded coarse sand and poorly sorted, angular gravel (15–55 cm), grading increasing to gravel, interpreted as increasing alluvial input and shoreline abandonment. One tufa clast was dated to 9430–9490 cal yr BP (AA97340). The uppermost section (70–80 cm) is composed of matrix-supported, non-calcareous fine sand with dispersed pebbles consistent with post-lake eolian deposition. Pedogenic carbonates showing Stages I to II morphology (Gile et al., 1966) cement the upper 30–35 cm of the section.

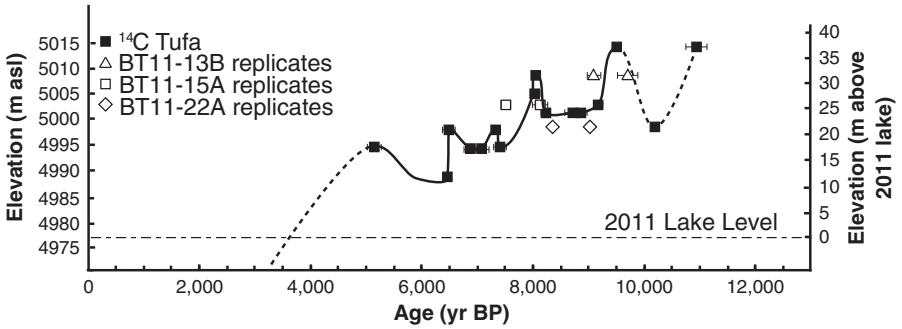


**Figure 5.** Summary of Baqan Tso lake level history. Replicate samples for shorelines BT11-13B, -15A, and -22A are in the open triangles, squares, and diamonds, respectively. Some error bars are smaller than their respective symbol.

https://doi.org/10.1016/j.yqres.2014.07.011 Published online by Cambridge University Press

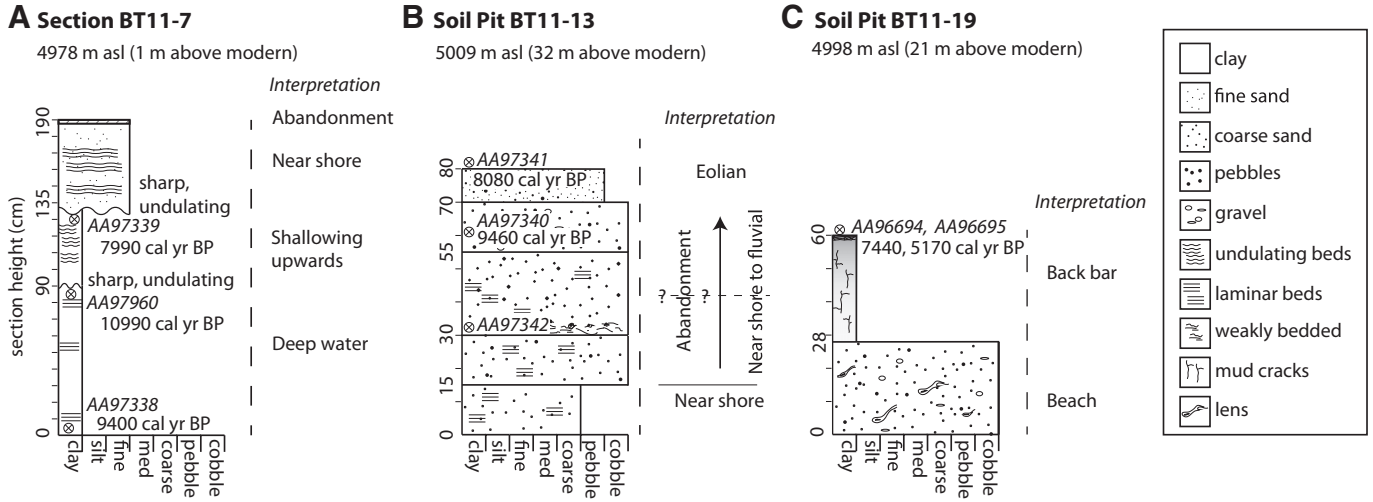


**Figure 6.** A stratigraphic section and soil pits from Baqan Tso (A) at BT11-7 (see Fig. 2), (B) at BT11-13 at the high altitude (5009 m, away from the lake) end of the Long Transect, and (C) Soil pit BT11-19 at the low altitude (4998 m, near the lake) end of the Long Transect.

Carbonate from this horizon produced an age of 2500–2750 cal yr BP (AA97342) unrelated to the lake record. A tufa clast taken from the top of the sequence dates to 8010–8160 cal yr BP (AA97341).

*BT11-19 (4998 m asl, 21 m above modern lake)*

Soil pit BT11-19 exposes what is probably another regressional sequence located lakeward of BT11-13 in the Long Transect (Fig. 2). The lowermost layer (0–28 cm) is composed of extremely hard, iron-stained, coarse sand and gravel interbedded with gray lenses of highly calcareous clay and fine sand, consistent with beach deposition (Fig. 3, Fig. 6). This grades upwards into a massive, highly calcareous clay (28–59 cm), and is capped by a very hard, white calcite with mud cracks (59–60 cm), representing lithoid tufa formation in a back-bar setting. Surface clasts collected in this context showed layering with the top and bottom of a clast dated to 7330–7550 (AA96695) and 5050–5300 (AA96694) cal yr BP, respectively.

*Lake history*

In general, Baqan Tso lake level was the highest in the early Holocene and decreased towards the mid-Holocene. Several sub-millennial lake-level oscillations are superimposed on this overall trend (Fig. 5). The oldest and the highest dated paleoshoreline lies at 5014 m (+37 m above modern). The lake stabilized around this elevation between 11.0 and 9.5 ka. At 10.2 ka, the lake may have fallen to 5001 m (+24 m above modern), although this single date could also result from reworking from a higher shoreline. The lake fell to 5004 m (+27 m above modern) between 9.4 and 9.2 ka, and stabilized around this elevation until 8.2 ka. The lake then rose sharply to 5009 m (+32 above modern) by 8.1 ka, and fell again to 4998 m (+21 m above modern) by about 7.4 ka. Between 7.4 and 6.5 ka lake level stabilized around 4997 and 5000 m (+20 to +23 m above modern), then dropped to 4993 m (+16 m above modern) within ≈100 yr (see Table 1). Lake level stabilized at this elevation until 5.9 ka, and then transgressed at 5.2 ka to 4999 m (+21 m above modern). There are no shorelines dated after 5.2 ka and it is likely that Baqan was near or below the modern lake level during the latter half of the Holocene.

It is possible that some of the sub-millennial oscillations we identify could actually be the result of reworking. To address this issue, we dated several different samples of lithoid-tufa from individual shorelines (Fig. 5, Table 1). These yielded a range of ages that we interpret as repeated occasions when the lake passed through the shoreline, precipitating additional lithoid-tufa. We favor this interpretation for three reasons. First, as a small lake in a nonglaciated basin, Baqan Tso is very sensitive to changes in hydroclimate and is likely to have had centennial or shorter interval lake-level oscillations through the Holocene resulting in multiple reoccupations of lake levels. Second, the dates show agreement at the same elevation in separate locations in both the Long and Short transects (Fig. 5). Lastly, the agreement between the Baqan Tso lake level record, and that of nearby Ngangla Ring Tso (Fig. 7; Hudson et al., 2014-in this issue), involving many more dates and sample localities than at Baqan Tso, argues against significant reworking affecting the lake level record.

## Hydrologic budget modeling

To quantify this hydrologic record for the Holocene, we have employed a coupled runoff and lake surface evaporation model to estimate the climatic conditions required to sustain the lake system at higher lake levels in the past. In closed-basin lake systems, the ratio of lake area to total basin area is physically related to the balance of lake inputs (precipitation and runoff) and outputs (evaporation). Modeling past precipitation using shorelines takes advantage of this physical relationship, which has been clearly demonstrated for Tibetan Plateau lakes (Hudson and Quade, 2013). We couple land runoff and lake evaporation models that have been previously validated for the conterminous the US and lake Nam Tso, near Lhasa, Tibet, respectively, to the Baqan Tso basin to simulate the precipitation required to sustain its modern, early Holocene, and mid-Holocene lakes.

*Model design and simplifying assumptions*

The basic hydrologic mass balance model for a closed-basin lake must balance inputs from direct precipitation on the lake and runoff to the lake with output through evaporation from the lake to maintain lake level at steady state and thus form a shoreline (Kutzbach, 1980):

$$P_{tot} \times a_W + R_L \times a_L = E_W \times a_W \quad (1)$$

where $P_{tot}$ is the total precipitation flux for the entire basin, $R_L$ is the total runoff flux for the basin land area, $E_W$ is the evaporation flux from the lake surface, and $a_W$ and $a_L$ represent the fractional area of the basin covered by water and land, respectively. The fractional lake area is expressed $a_W = A_W / (A_W + A_L)$, where $A_W$ refers to the area of the lake and $A_L$ refers to the area of the basin excluding the lake.

https://doi.org/10.1016/j.yqres.2014.07.011 Published online by Cambridge University Press

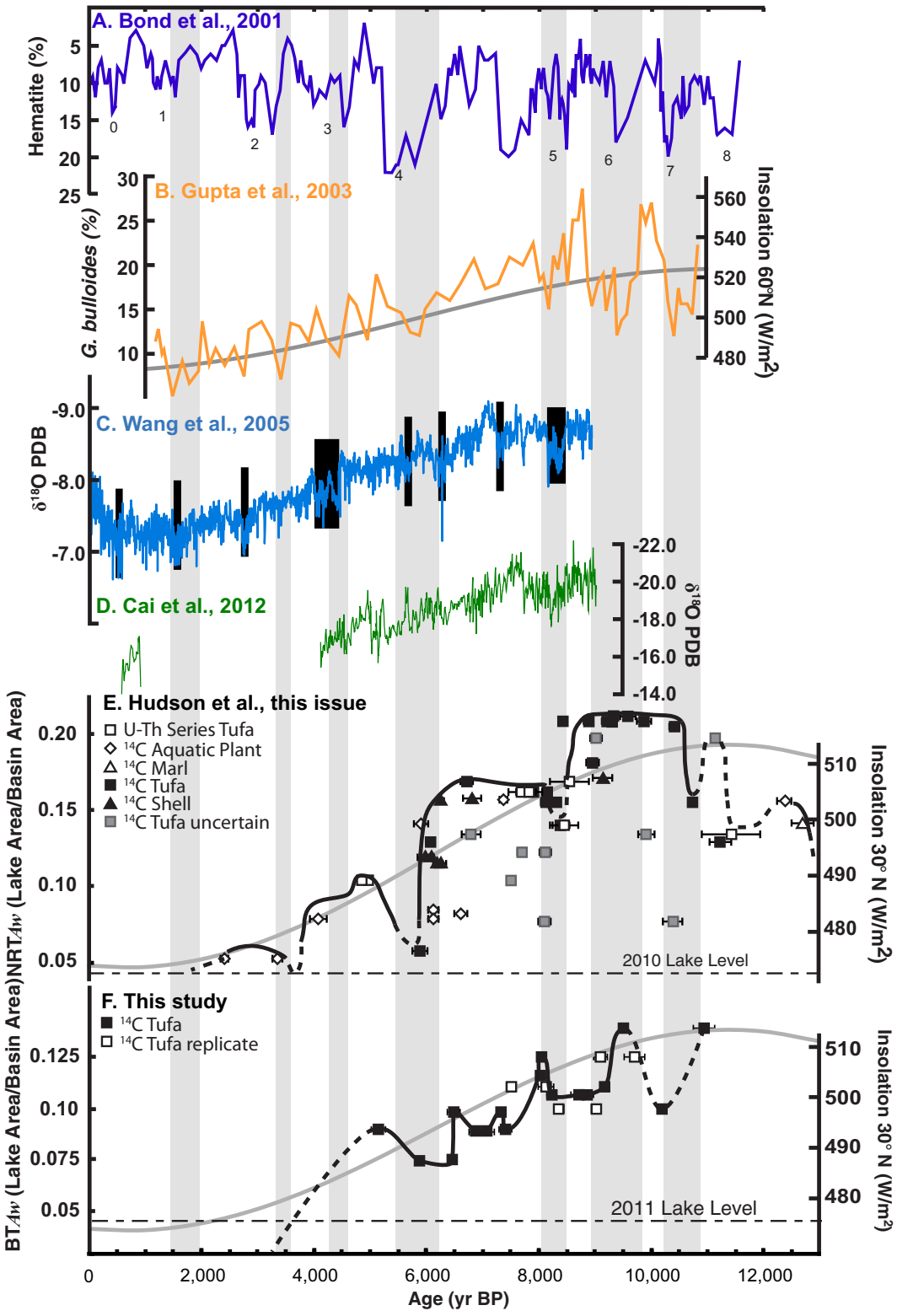


**Figure 7.** Comparison of marine and speleothem records to Baqan Tso and Ngangla Ring Tso lake levels: (A) Hematite abundance in North Atlantic core MC50-VM29-191 (Bond et al., 2001), (B) abundance of cold water foram, *G. bulloides* from the Oman margin (ISM strength proxy) (Gupta et al., 2003) and June 60°N summer insolation, (C) Dongge Cave speleothem 'DA' calcite $\delta^{18}O$ record — black vertical bars denote weak monsoon events interpreted in this record (Wang et al., 2005), (D) $\delta^{18}O$ (PDB) values of speleothem calcite from Tianmen Cave (Cai et al., 2012), (E) Ngangla Ring Tso lake-level curve (Hudson et al., 2014-in this issue) and June 30°N insolation, and (F) the Baqan Tso lake-level curve (this study) and June 30°N insolation (Berger and Loutre, 1991). Vertical gray bars indicate intervals of weak Indian Summer Monsoon identified by Gupta et al. (2003).

The values of $a_W$ and $a_L$ for each reconstructed lake level of known age were calculated using ArcGIS software on an equal area map projection for the Baqan Tso drainage basin, and the hydrologic budget model focuses on acquiring estimates for $E_W$ and $R_L$ based on a combined lake-specific surface heat budget model (Haginoya et al., 2009) and basin-specific runoff model (McCabe and Markstrom, 2007).

The Baqan Tso basin is extremely remote, and the western Tibetan Plateau has few meteorological stations. Furthermore, temperature

https://doi.org/10.1016/j.yqres.2014.07.011 Published online by Cambridge University Press

and precipitation are locally variable depending upon elevation and distance from the plateau margin due to the complex topography and dry climate in the rain shadow of the Himalaya and Gangdise mountain ranges. Therefore, several assumptions, detailed in the model descriptions below, are required to estimate accurate modern climate parameters for the Baqan Tso basin using available climate data.

### *Land-specific model for determination of $R_L$*

The Thornthwaite basin model is a monthly water-balance model that has been calibrated to and validated with runoff from streamflow-gage sites in the conterminous United States (Thornthwaite, 1948; McCabe and Markstrom, 2007). Temperature and annual precipitation ranges in Tibet are similar to the western U.S., so we use this model to calculate runoff from the land surface of the basin. The full model is not described here, but briefly, the model requires inputs for air temperature, $T_a$, precipitation, $P$, and a specified soil-moisture storage capacity (*STC*), which are used to estimate runoff from calculations of potential evapotranspiration (*PET*), actual evapotranspiration (*AET*), whether precipitation falls as snow ($P_{snow}$) or rain ($P_{rain}$), whether snow melts (*SM*) or persists on the surface (*snostor*), the reservoir of soil-moisture storage (*SWremain*), direct runoff (*DRO*) and surplus runoff (*RO*) from the soil. Direct runoff is water that immediately leaves the soil (e.g., precipitation falling on impervious surfaces) while surplus runoff is water in excess of the soil-moisture storage capacity (*STC*) that leaves the soil (e.g., spring snowmelt). Total runoff ($R_L$) is defined as the sum of direct runoff and surplus runoff from the soil. An example year of calculation for the Baqan Tso basin surface is presented in Table 2.

### *Calculating modern $R_L$ for the Baqan Tso basin*

Monthly average data for precipitation and air temperature were taken from the nearby (≈150 km away) Gerze weather station (station 55248) for the years 1973–2006 (Fig. 1). Soil-moisture storage capacity (*STC*) for Baqan Tso was calibrated from modern lake size and weather data as 415 mm, which is higher than the 60–309 mm *STC* range considered by Wolock and McCabe (1999) for the conterminous US. Air temperature was elevation-corrected using a lapse rate of 7°C/km. For the modern model input of precipitation, we retained the seasonal cycle of Gerze rainfall and matched the 240 mm/yr TRMM estimate for the Baqan Tso basin by increasing each monthly value by a factor of 1.40 (Fig. 4).

### *Lake surface heat budget model for determination of $E_W$*

We use the single layer lake-specific heat-balance model of Haginoya et al. (2009), developed and calibrated for Nam Tso near Lhasa, Tibet, to estimate $E_W$ for Baqan Tso. This daily heat balance model is similar to those used by other researchers (e.g., Hostletler and Bartlein, 1990 as applied in the region by Morrill, 2004 and Li and Morrill, 2010) and balances downward fluxes from incoming solar radiation at the lake surface and atmospheric long wave radiation with upward fluxes of longwave radiation from the lake, sensible heat exchange, and latent heat by evaporation. The downward radiation flux input to a lake can be written as:

$$R^{\downarrow} = (1-a)\,S^{\downarrow} + \varepsilon L^{\downarrow}. \tag{2}$$

Here, $R^{\downarrow}$ represents the downward radiation flux, $\alpha$ is the lake surface albedo, $S^{\downarrow}$ is incoming solar radiation, $\varepsilon$ is surface emissivity, and $L^{\downarrow}$ is the downward long wave radiation flux from the atmosphere to the surface.

The heat balance equation for a lake can be written as

$$R^{\downarrow} - G_0 = \varepsilon\sigma T_s^4 + H + lE \tag{3}$$

where $G_0$ is the heat flux of conduction from the lake surface into the water or ice below, $\sigma$ is the Stefan–Boltzmann constant ($5.67 \times 10^{-8}$ W m$^{-2}$ K$^{-4}$), $T_s$ is the calculated surface temperature of water or ice, and $H$ and $lE$ are the sensible and latent heat fluxes, respectively, at the lake surface.

The values for $G_0$, $H$, and $lE$, were calculated as follows:

$$G_0 = dcp(\partial T_s/\partial t) \tag{4}$$

$$H = cpPaCHU(Ts - Ta) \tag{5}$$

$$lE = l\rho a\beta CHU(q_{SAT}(Ts) - qa). \tag{6}$$

For calculating $G_0$, $d$ is the depth of the mixed layer (epilimnion) or maximum freezing depth of the lake, $c$ is the specific heat of water or ice, $\rho$ is the density of water or ice, and $\partial Ts/\partial t$ is the variation of surface temperature with time $t$. For calculating $H$, $cp$ is the specific heat of air, $\rho a$ is the density of air, $CH$ is the bulk transfer coefficient, $U$ is wind speed, and $Ta$ is air temperature.

**Table 2**
Example simulation for Thornthwaite (1948) land-specific model.

| Month | $T_a$ (°C)[a] | $P_{rain}$ mm[b] | $P_{snow}$ mm | *snostor* mm | *DRO* mm[c] | *RO* mm | *SM* mm | *PET* mm | *AET* mm | *SWremain* mm | *ROtotal* mm |
|---|---|---|---|---|---|---|---|---|---|---|---|
| Jan | −15.4 | 0 | 0 | 11 | 0.0 | 0.0 | 0.0 | 7.1 | 2.8 | 0.0 | 0.0 |
| Feb | −14.1 | 0 | 4 | 15 | 0.0 | 0.0 | 0.0 | 7.2 | 2.7 | 0.0 | 0.0 |
| Mar | −7.8 | 0 | 3 | 18 | 0.0 | 0.0 | 0.0 | 12.2 | 4.6 | 0.0 | 0.0 |
| Apr | −3.0 | 0 | 2 | 20 | 0.0 | 0.0 | 0.0 | 16.6 | 5.9 | 0.0 | 0.0 |
| May | 0.1 | 1 | 2 | 22 | 0.0 | 0.0 | 2.8 | 21.6 | 9.5 | 0.0 | 0.0 |
| Jun | 5.0 | 49 | 0 | 19 | 2.4 | 0.0 | 9.6 | 29.1 | 29.1 | 0.0 | 2.4 |
| Jul | 8.2 | 68 | 0 | 10 | 3.4 | 0.0 | 4.8 | 37.4 | 37.4 | 0.0 | 3.4 |
| Aug | 8.6 | 44 | 0 | 5 | 2.2 | 0.0 | 2.4 | 38.6 | 38.6 | 0.0 | 2.2 |
| Sep | 4.7 | 1 | 0 | 2 | 0.0 | 0.0 | 1.2 | 29.3 | 16.4 | 0.0 | 0.0 |
| Oct | −1.4 | 0 | 0 | 1 | 0.0 | 0.0 | 0.0 | 20.5 | 9.9 | 0.0 | 0.0 |
| Nov | −12.3 | 0 | 3 | 5 | 0.0 | 0.0 | 0.0 | 10.0 | 4.5 | 0.0 | 0.0 |
| Dec | −14.6 | 0 | 0 | 5 | 0.0 | 0.0 | 0.0 | 8.8 | 3.8 | 0.0 | 0.0 |
| Annual | −3.5 | 163 | 15 | 133 | 8 | 0 | 21 | 238 | 165 | 0 | 8 |

Inputs are $T_a$: air temperature and $P_{(rain,snow)}$: precipitation. Model parameters are *snostor*: snow storage, *DRO*: direct runoff, *RO*: soil water runoff, *SM*: snowmelt, *PET*, potential evapotranspiration, *AET*: actual evapotranspiration, *SWremain*: soil-moisture storage, and *ROtotal*: total runoff.

[a] Based on Gerze $T_a$ and adjusted for a lapse rate of 7°C/km.

[b] Has same seasonality as Gerze weather station data but is multiplied by 1.36 to match annual TRMM precipitation estimate.

[c] 5% of $P_{rain}$.

https://doi.org/10.1016/j.yqres.2014.07.011 Published online by Cambridge University Press

**Table 3**
Example simulation for Haginoya et al. (2009) lake-specific model.

| Month | $P$ hPa[a] | $T_a$ (°C)[a,c] | $RH$ %[b,d] | $U$ m s$^{-1}$[b] | $S\downarrow$ W m$^{-2}$[b] | $L\downarrow$ W m$^{-2}$ | $\alpha$[b] | $H$ W m$^{-2}$ | $E$ mm |
|---|---|---|---|---|---|---|---|---|---|
| Jan | 566.2 | −16.2 | 29.25 | 5.7 | 149 | 175 | 0.17 | 14 | 33 |
| Feb | 566.6 | −13.9 | 22.25 | 3.1 | 196 | 181 | 0.55 | −3 | 17 |
| Mar | 568.5 | −10.3 | 32.25 | 3.4 | 234 | 193 | 0.54 | 1 | 27 |
| Apr | 571.3 | −4.3 | 29.25 | 3.7 | 261 | 213 | 0.38 | 8 | 57 |
| May | 572 | −0.2 | 32.25 | 3.4 | 280 | 229 | 0.06 | 30 | 94 |
| Jun | 572.4 | 7.0 | 42.25 | 3.4 | 273 | 238 | 0.06 | 12 | 82 |
| Jul | 573 | 7.9 | 57.25 | 3.2 | 246 | 254 | 0.06 | 14 | 78 |
| Aug | 573.9 | 7.0 | 65.25 | 2.9 | 212 | 253 | 0.06 | 17 | 71 |
| Sep | 574 | 4.9 | 64.25 | 3.4 | 211 | 241 | 0.06 | 23 | 79 |
| Oct | 573.6 | −2.0 | 28.25 | 3.4 | 197 | 221 | 0.06 | 36 | 97 |
| Nov | 571.5 | −11.1 | 18.25 | 3.4 | 166 | 189 | 0.06 | 50 | 73 |
| Dec | 568.8 | −15.1 | 20.25 | 3.8 | 146 | 178 | 0.06 | 21 | 34 |
| Annual | 571.0 | −3.9 | 37 | 3.6 | 214 | 214 | 0.18 | 19 | 742 |

$P$: pressure, $T_a$: air temperature, $RH$: relative humidity, $U$: wind speed, $S\downarrow$: global solar radiation, $L\downarrow$: downward longwave radiation, $\alpha$: albedo, $T_s$: surface temperature, $H$: sensible heat flux, $E$: evaporation.
[a] Data from Gerze weather station.
[b] Data from Haginoya et al. (2009).
[c] Based on Gerze $T_a$ and adjusted for a lapse rate of 7°C/km.
[d] Corrected with the modern $RH$ versus $P_{tot}$ relationship (Fig. 7a).

For calculating $lE$, $l$ is the latent heat of vaporization, $\beta$ is evaporation efficiency, $qSAT(Ts)$ is specific humidity at saturation for a particular $Ts$, and $qa$ is the specific humidity of the air above the lake surface.

The latent heat of melting is considered when the water temperature reaches 0°C. At this point, a surface ice layer is assumed to immediately reach its maximum freezing depth ($d_{ice}$) of 0.6 m, based on measurements for Nam Tso (Haginoya et al., 2009). After reaching the maximum freezing depth, the temperature of the ice layer changes uniformly with depth according to the surface energy balance.

Running the model requires calculating $G_i$ at a time step $\Delta t$ (86,400 s = 1 day). At $t = 0$, we assume $T_{s0} = T_a$. For each subsequent time step $i$, where $t = i \times \Delta t$, $G_{0i}$ and $T_{si}$ are calculated as

$$Go_i = (1-a)S^{\downarrow} + \varepsilon L^{\downarrow} - \varepsilon\sigma {T_{si-1}}^4 - H - lH \quad (7)$$

$$T_{si} = T_{si-1} + (\Delta t G_{0i}/dcp). \quad (8)$$

The lake-specific model requires climate input data for daily mean surface air temperature $Ta$ (K or °C), daily mean vapor pressure $e$ (hPa), daily mean wind speed $U$ (m s$^{-1}$), daily mean solar radiation flux $S^{\downarrow}$ (W m$^{-2}$), and albedo. Saturated vapor pressure of the lake and air is calculated from the temperature of the lake ($Ts$) and air ($Ta$), respectively (modified Clausius Clapeyron equation). These variables and $RH$ are then used to calculate vapor pressure, the specific humidity of air ($q$), and the specific humidity at saturation ($qSAT(Ts)$). Downward longwave radiation is calculated from $Ta$, $RH$, and saturation vapor pressure (for Ta > 0°C, Brutsaert, 1975; for Ta < 0°C, Idso, 1981). An example year of calculation for Baqan Tso for is presented in Table 3.

*Calculating evaporation from Baqan Tso*

We estimated conditions at Baqan Tso using data from the Gerze station (station 55248, Fig. 1) supplemented by data from Nam Tso (Haginoya et al., 2009). $T_a$ and relative humidity ($RH$) were compiled from Gerze. Air temperature was modified by a lapse rate of 7°C/km as before. We additionally characterized the modern Tibetan Plateau with six weather stations (Li et al., 2010, Fig. 1), and published data from Nam Tso (Haginoya et al., 2009). The modern climate system exhibits a relationship between relative humidity and total precipitation ($r^2 = 0.73$) (Fig. 8). We used this relationship and the ≈65 mm/yr precipitation difference between Gerze and Baqan Tso to approximate that mean $RH$ at Baqan Tso is 1.08 times greater than at Gerze. We assumed $U$, $S^{\downarrow}$, and $\alpha$ at Baqan Tso were similar to Nam Tso (Haginoya et al., 2009) because the two lakes are at similar latitudes and altitudes (Table 3). The depth of the mixing layer ($d$) was set at 10 m, as at Nam Co (Haginoya et al., 2009), but decreasing $d$ to 5 m only changes precipitation estimates by ≈5%. The bulk transfer coefficient was set to 0.002 for Ta < 0°C (Kondo and Yamazawa, 1986) and 0.0014 for Ta > °0 C (Hicks, 1972). Monthly data averaged over 2006–2008 was available for variables from Haginoya et al. (2009) so the model was run with repeats of this single year of averaged data to acquire a value for $E_W$ independent of starting conditions. Monthly data from both sources were expanded to daily data by substituting the monthly average value for each day so that the model could run at a daily time-step. The model is not dependent on initial conditions after about a half year of calculations (Haginoya et al., 2009).

*Modern basin precipitation estimate*

Overall basin precipitation ($P_{tot}$) is known independently for the modern basin and can be used to assess the model's accuracy. Forcing the runoff model with $P_{tot}$ matching the TRMM value of 240 mm/yr

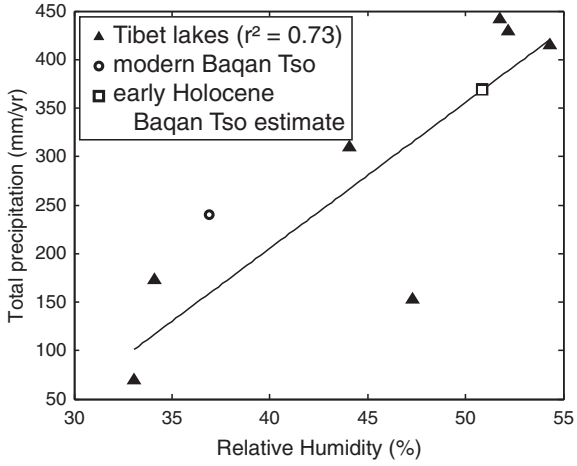


**Figure 8.** Modern climate characteristics of eastern and western Tibet. Modern relative humidity ($RH$) versus total observed precipitation ($P_{tot}$) for Tibet (filled triangles). Data are from weather stations 55228, 55248, 55279, 55294, 55299, and 55437 (Fig. 1) and published data from Nam Tso (Haginoya et al., 2009). The open circle represents the modern TRMM precipitation estimate at Baqan Tso. The open square represents the modeled early Holocene paleo-rainfall and humidity at Baqan Tso.

https://doi.org/10.1016/j.yqres.2014.07.011 Published online by Cambridge University Press

yields a total runoff flux from the land of 17 mm/yr. The lake model gives a modern evaporation rate from the lake of 700 mm/yr, comparable in magnitude to Nam Tso and other modeled lakes in eastern China and Japan (Haginoya et al., 2009 and citations therein). Using Eq. (1) to calculate $P_{tot}$ for the modern lake returns a steady-state estimate of 240 mm/yr for modern conditions (Table 4). This compares closely to the TRMM estimate of 240 mm/yr, indicating that our model approach is representative of the basin hydrologic budget.

*Modeling the Holocene precipitation history for the Baqan Tso basin*

In solving the model for the early Holocene lake level record, we must account for changes in solar radiative (or insolation) inputs for the Haginoya model. Berger and Loutre (1991) calculated monthly values every 1000 yr at 10° latitude intervals. We calculated monthly insolation values at Baqan Tso's latitude by interpolating between Berger and Loutre's (1991) values for each lake level age in the record (Fig. 9a). The percent change in mean monthly insolation from modern to the early Holocene (11.5 ka) was applied to the modern monthly $S^{\downarrow}$ values from Nam Tso to capture the increased seasonality of insolation. This approach assumes that changes in cloud cover from the early Holocene to present were minimal. The larger precipitation required to sustain the early Holocene lake was likely associated with more cloud cover, and we incorporate possible cloud cover effects on $S^{\downarrow}$ through error bars (see below).

Although seasonality was greater in the early Holocene as compared to today, there was only a modest increase in mean annual insolation ($\approx$1.3% at Baqan Tso latitude). Nearly equal increases in summer insolation and decreases in winter insolation suggest that mean annual temperature (MAT) during the early Holocene at Baqan Tso is not likely to have been significantly greater than present. Additionally, pollen-based temperature reconstructions from central and eastern Tibet lake sediment cores suggest a MAT increase of $\approx$1–3°C for the early Holocene (e.g., Herzschuh et al. 2006a; Kramer et al., 2010). We therefore assume a MAT increase of 2°C at Baqan Tso for the highest insolation period during the early Holocene (11.5 ka) and incorporate errors of $\pm$1°C below. We then adjust MAT for each shoreline age following percent change in mean insolation through time between modern and 2°C (Fig. 9B), assuming constant seasonality for temperature throughout the simulation. Mean monthly temperatures are unlikely to deviate more than a few degrees from their current values, and as calculated below, a 1°C error in MAT results in a $\approx$5% change in $P_{tot}$. We have no estimates for wind speed or air pressure during the Holocene, but since the lake model is relatively insensitive to these variables, we keep them the same throughout for simplicity.

Because the Thornthwaite runoff model requires $P_{tot}$ as an input for each dated lake level, the model must be solved iteratively to find a solution that satisfies Eq. (1). We have no data on how relative humidity changed through the Holocene, which is problematic because large changes to *RH* can cause precipitation estimates to be significantly different. We reconstruct the Holocene record of $P_{tot}$ and *RH* at Baqan Tso using some assumptions about early Holocene climate. Terrestrial pollen records show that western Tibet in the early Holocene was floristically similar to eastern Tibet today (Demske et al., 2009, Kramer et al., 2010). We therefore assume that early Holocene climate in western Tibet was somewhat warmer and wetter, and had similar precipitation seasonality (i.e., summer monsoon-dominated) to modern central and eastern Tibet. With these assumptions, we use the modern Tibetan Plateau relationship between relative humidity and total precipitation in a basin (Fig. 8) to estimate *RH* and $P_{tot}$ values in the past.

The modern relationship between *RH* and $P_{tot}$ forces the paleoprecipitation estimates for the early Holocene. Given the fractional water and land areas, $a_W$ and $a_L$, for the early Holocene shoreline and the above input variables, we iteratively solve for the $RH/P_{tot}$ pair required for hydrologic balance at each dated lake level. We solve for this pair by finding the value of *RH* that matches the precipitation value from the modern regression to that required to balance the coupled model.

Solving the hydrologic balance using Eq. (1) for the early Holocene lake highstand requires 140 mm/yr or a 55% increase in precipitation over modern, and a 37% increase in *RH*. Lake evaporation (*Ew*) is estimated to be 690 mm/yr and total runoff ($R_L$) is estimated to be 62 mm/yr (Table 4). These climate conditions explain the 4.3× lake area expansion during the early Holocene.

An identical approach to paleorainfall reconstruction can be taken for other Holocene shorelines below the early Holocene high shoreline (5043 m) and the modern lake (4977 m). The $P_{tot}/RH$ values estimated for all of the Holocene shorelines range between 300 and 380 $\pm$ 29–57 mm/yr (Fig. 10).

*Model sensitivity and error estimates*

We rate variable sensitivity by the magnitude of change in $P_{tot}$ resulting from the likely error in an input variable (see below, Table 5). Using this standard, the model is most sensitive to *RH*, with a 10% change ($\approx$3% RH) giving a 7% change in $P_{tot}$. The model is less

**Table 4**
Paleo-precipitation ($P_{tot}$) estimated for various shoreline elevations.

| Shoreline age | Shoreline elevation | $R_L$ mm/yr | $a_L$ | $E_W$ mm/yr | $a_W$ | $P_{tot}$ mm/yr | $P_{tot}$ change from modern mm/yr |
|---|---|---|---|---|---|---|---|
| Modern (2011) | 4977 | 18 | 0.963 | 701 | 0.037 | 240 | 0 |
| 5170 | 4998 | 41 | 0.910 | 726 | 0.090 | 310 | 70 |
| 5930 | 4993 | 36 | 0.924 | 737 | 0.076 | 300 | 60 |
| 6490 | 4993 | 36 | 0.924 | 744 | 0.076 | 305 | 65 |
| 6520 | 5000 | 44 | 0.904 | 743 | 0.096 | 320 | 80 |
| 6900 | 4997 | 41 | 0.913 | 748 | 0.087 | 315 | 75 |
| 7110 | 4997 | 42 | 0.913 | 751 | 0.087 | 320 | 80 |
| 7360 | 5000 | 46 | 0.904 | 755 | 0.096 | 330 | 90 |
| 7440 | 4998 | 43 | 0.910 | 757 | 0.090 | 325 | 85 |
| 8080 | 5006 | 46 | 0.887 | 688 | 0.114 | 330 | 90 |
| 8080 | 5009 | 49 | 0.878 | 687 | 0.122 | 340 | 100 |
| 8240 | 5003 | 43 | 0.895 | 690 | 0.105 | 325 | 85 |
| 8780 | 5003 | 43 | 0.895 | 694 | 0.105 | 330 | 90 |
| 8890 | 5003 | 43 | 0.895 | 695 | 0.105 | 330 | 90 |
| 9210 | 5004 | 44 | 0.892 | 697 | 0.108 | 330 | 90 |
| 9540 | 5014 | 54 | 0.863 | 697 | 0.137 | 355 | 115 |
| 10,230 | 5001 | 41 | 0.901 | 705 | 0.099 | 330 | 90 |
| 10,980 | 5014 | 54 | 0.863 | 704 | 0.137 | 360 | 120 |
| early Holocene | 5023 | 64 | 0.837 | 701 | 0.163 | 380 | 140 |

https://doi.org/10.1016/j.yqres.2014.07.011 Published online by Cambridge University Press

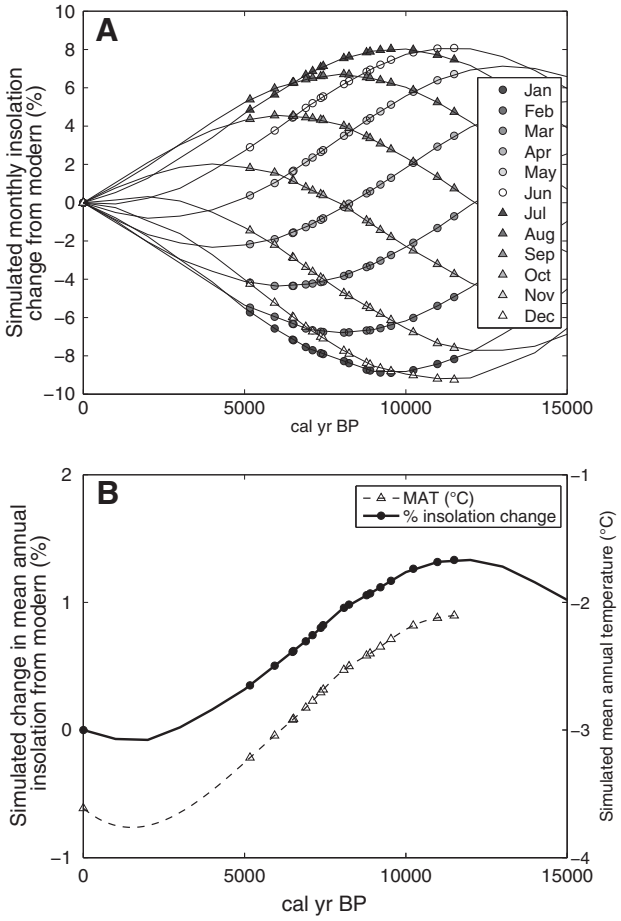


**Figure 9.** (A) Percentage change in mean monthly solar insolation at Baqan Tso through time as interpolated from simulated 1000-yr intervals by Berger and Loutre (1991). Each marker represents a single month's percentage change from modern for a dated shoreline at Baqan Tso. (B) Percentage change in mean annual solar insolation (solid line) and simulated mean annual temperature (dashed line) at Baqan Tso through time. Mean annual temperature curve is weighted to exactly follow the relative change in mean annual insolation through time. Markers represent the percentage change for dated shorelines' mean annual solar insolation (filled circles) and mean annual temperature (open triangles) for a dated shoreline at Baqan Tso.

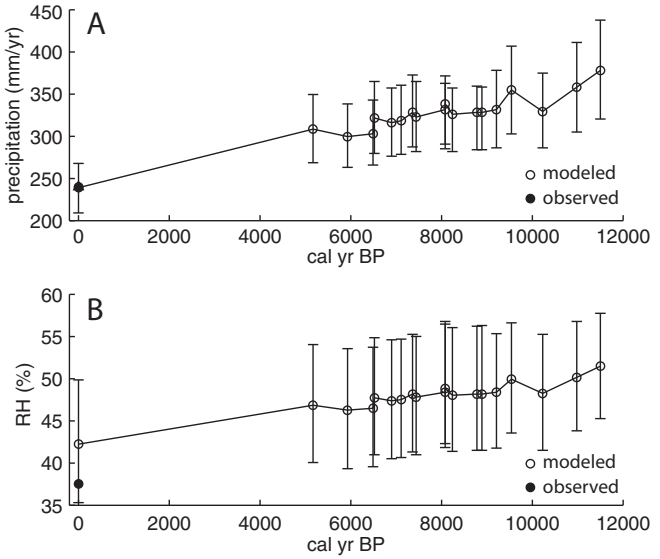


**Figure 10.** Simulation of Holocene climate of Baqan Tso (A) simulation of rainfall at Baqan at the dated shorelines. Open circles are modeled rainfall and the filled circle is the modern TRMM rainfall estimate for Baqan Tso Basin (overlaps with the modeled modern rainfall estimate). (B) Simulation of relative humidity at Baqan at the dated shorelines. Open circles are modeled relative humidity. The filled circle is the modern Gerze station relative humidity estimate corrected with the modern RH versus $P_{tot}$ relationship (Fig. 8) for Baqan Tso basin. Error bars in both plots are intended to represent the reasonable maximum amount of error for the simulated precipitation or relative humidity value.

sensitive to *Ta*, with a 1°C change giving a 5% change in $P_{tot}$, and to *U*, with a 10% change ($\approx$0.3 m s$^{-1}$) giving a 2% change in $P_{tot}$. It is insensitive to $S^{\downarrow}$, with a 0.5% change ($\approx$7 W m$^{-2}$) giving a $\approx$0.5% change in $P_{tot}$ and to $p_{air}$, with a 10% change ($\approx$60 hPa) giving a 0.5% change in $P_{tot}$. The model is insensitive to small changes in the modern $P_{tot}$ vs. *RH* regression, with an added 30 mm/yr $P_{tot}$ error yielding a 0.5% change in $P_{tot}$ and a 10% change in *RH* values yielding a 0.5% change in $P_{tot}$. An example of model sensitivity at the highstand shoreline conditions is provided in Table 5.

Error in *RH* and *U* can have an appreciable impact on precipitation estimates because these variables are likely to have been substantially different during the early Holocene. This is especially true for relative humidity, given the modern *RH* vs. $P_{tot}$ relationship that forces the coupled model. Additionally, relatively small changes in temperature and solar insolation strongly influence the modeled increase in precipitation for Baqan Tso for the early Holocene model scenario. However, the effects of changes in temperature and solar insolation are countered by a large increase in humidity using our modern station-based approach (Fig. 8). This scenario is reasonable, given that lower early Holocene ablation rates, due to higher cloud cover and humidity, have been suggested as a mechanism for glacier advances in Tibet (Rupper et al., 2009). However, the large required *RH* changes also highlight the importance of quantifying the impact of uncertainty in input variables on the final precipitation estimate.

To account for error in paleorainfall estimates due to uncertainties in input variables, we have calculated their associated errors. These are meant to reflect the largest realistic error associated with each precipitation estimate (Fig. 10A, Table 5). We estimated errors using two scenarios: a 'wet' scenario where all input variables were changed to require increased precipitation to balance Eq. (1) at a given shoreline and a 'dry' scenario where all input variables were changed to require decreased precipitation to balance Eq. (1). Percent error increases to input parameters were multiplied by the mean annual value and the calculated error was then added as a flat increase to each monthly value (i.e., seasonality remained unchanged). *RH*, *U* and $p_{air}$ were changed by $\pm$10%, $T_a$ was changed by $\pm$1°C, and $S^{\downarrow}$ was changed by $\pm$0.5% to bound error estimates by realistic maximum errors due to uncertainty in seasonality and the mean annual value of variables. For the 'wet' scenario, *U*, *Ta*, and $S^{\downarrow}$ were increased and *RH* and $p_{air}$ were decreased to require a larger precipitation flux. Increasing *Ta* by an

**Table 5**
Upper bounding error calculations at highstand shoreline.

| Input variable | Change | Units | Modeled $P_{tot}$ | % change in $P_{tot}$ |
|---|---|---|---|---|
| None | – | – | 378 | 0.0 |
| *RH* | −10 | % | 402 | 6.4 |
| *Ta* | 1 | °C | 396 | 4.7 |
| *U* | 10 | % | 387 | 2.3 |
| $p_{air}$ | −10 | % | 380 | 0.6 |
| *Rsw* | 0.5 | % | 379 | 0.3 |
| modern *RH* vs. $P_{tot}$ regression — *RH* | −10 | % | 379 | 0.3 |
| modern *RH* vs. $P_{tot}$ regression — $P_{tot}$ | 30 | mm/yr | 378 | 0.1 |
| All — the 'wet' scenario | As above | – | 435 | 15.2 |

Note that inputs are changed by different amounts to reflect realistic error in each variable and allow comparison of potential error between inputs.

https://doi.org/10.1016/j.yqres.2014.07.011 Published online by Cambridge University Press

additional 1°C means the upper error bound for the early Holocene highstand incorporates a total MAT increase of 3°C. To add error to the modern *RH* vs. $P_{tot}$ relationship, modern $P_{tot}$ data points were changed by ±30 mm/yr, *RH* data points were changed by ±10%, and the modern *RH* vs. $P_{tot}$ relationship was recalculated before running the error estimate. For the 'wet' scenario, modern $P_{tot}$ data points were increased and *RH* data points were decreased. Although neither of these inputs has a large effect on the final modeled $P_{tot}$, changing them varies *RH* values used to model $P_{tot}$ substantially (3–5% for each). This approach allows us to better incorporate the scatter in measured *RH* values around those values predicted by the modern regression ($r^2 = 0.73$), which is evident for the modern system (Fig. 10B).

The intent of these error estimates is to present a graphical sense of model sensitivity, as well as to provide realistic maximum magnitudes of error on each precipitation estimate. Upper and lower bounding error bars are slightly different for each shoreline because the model responds differently to input changes each direction (Fig. 10). Errors in our precipitation estimates (Fig. 10A) are estimated to be ±29–57 mm/yr (±12–15%), with the ±10% *RH* and ±1°C $T_a$ each composing a third of the total error. Error in *RH* (Fig. 10B) is ±12–17%, and is primarily the result of the imperfect ($r2 = 0.73$) fit of modern *RH* to $P_{tot}$. Additionally, because we have assumed constant seasonality, estimates of the maximum error associated with climate variable uncertainty provide assessments of the largest reasonable effects of changing seasonality (Fig. 10).

## Discussion

### *Regional significance*

Our reconstruction of lake-level changes from Baqan Tso is very similar to other local and regional records of paleohydrologic change from Tibet (Fig. 7). Baqan Tso was deepest during the early Holocene, steadily contracted towards the present, and was likely near in size or smaller than the present lake through the last 5000 yr. The Holocene drying trend is also seen locally at nearby Ngangla Ring Tso, with the most significant lake regression occurring after 6.0 ka, consistent with Baqan Tso (Hudson et al., 2014-in this issue) (Figs. 1, 7). The Baqan Tso record additionally contains evidence of sub-millennial oscillations that are also recorded at Ngangla Ring Tso, at approximately 6.5 ka, 7.5 ka, 9.0 ka and possibly 10.0 ka. Agreement of these events with the NRT record suggests that sub-millenial scale lake level changes interpreted in the Baqan Tso record can be reliably resolved in the shoreline chronology.

An early Holocene precipitation and/or hydrologic maximum with gradual drying through the Holocene is evident in the majority of other climate records from Tibet (e.g. Van Campo and Gasse, 1993; Gasse et al., 1996; Herzschuh et al., 2006b; Morrill et al., 2006). The early Holocene maxima are likely linked to a warmer, as well as wetter, climate during the early Holocene as seen in regional lake and pollen records (Gasse et al., 1996; Demske et al., 2009; Wünneman et al., 2010; Hudson et al., 2014-in this issue). These records also show an overall decrease in precipitation and temperature towards the present, although the exact timing of peak wetness in Asia occurs anywhere from early- to mid-Holocene (Herzschuh, 2006).

The hydrologic history derived from Baqan Tso and Ngangla Ring Tso lake levels and other Tibetan Plateau proxy records is similar to the pattern apparent in regional ocean cores (Gupta et al., 2003) and cave $\delta^{18}O$ records within and outside the plateau (e.g., Dykoski et al., 2005; Wang et al., 2005; Cai et al., 2012) (Fig. 7). The overall rainfall decrease inferred at Baqan Tso and other locations is thought to be caused by decreasing Northern Hemisphere solar insolation controlling rainfall amount or source area variability in the East Asian and Indian Monsoons (Fleitmann et al., 2003; Overpeck et al., 1996; Wang et al., 2008). The abrupt 10.0, 7.5, and 6.5 ka lake-level regressions at Baqan Tso are also coincident with inferred reductions in Indian Summer Monsoon-associated upwelling, evident in the abundance of the cold water foram *Globigerina bulloides* along the Oman margin (Gupta et al., 2003), and with temperature- and/or precipitation induced glacial advances in Tibet (Yi et al., 2008; Owen, 2009; Seong et al., 2009). These events are coincident with large increases in hematite abundance in the North Atlantic, indicating an atmospheric teleconnection with monsoon rainfall amount may exist (Bond et al., 2001).

### *Model implications for Holocene monsoon climate*

These local, regional, and global connections show that the changes in lake size and precipitation at Baqan Tso are representative of paleohydrologic changes of lake systems across the western Tibetan Plateau. Workers at other lakes have suggested increased glacial meltwater flux as a driver of lake level change in Tibet (e.g. Li et al., 2001; Kong et al., 2007). However, Hudson and Quade (2013) show that in western Tibet basins, early Holocene increases in lake area are similar independent of whether or not a basin is glaciated, indicating that changing precipitation, not glacial meltwater flux, is the dominant water source for lake level oscillations. In particular, we stress that changes in glacial meltwater flux cannot explain lake level oscillation at Baqan Tso because the basin was not glaciated at any point during the Holocene. This study significantly expands our understanding of Holocene climate change on the Tibetan Plateau because it is, to our knowledge, the first quantitative precipitation estimate for the plateau.

The model used here to quantify the effects of climate change on Holocene lake levels at Baqan Tso can be applied to many other lakes in Tibet. Tibet has more closed-basin lakes than anywhere else in the world, many of which are not currently or formerly glaciated (Hudson and Quade, 2013), which makes it an ideal location for model reconstructions across a wide area. Furthermore, Tibet can be divided into eastern and western regions across a dividing line at ≈86°E based on lake expansions during the early Holocene (see Hudson and Quade, 2013). During the early Holocene, lake areas in eastern Tibet expanded much less (1.1–2.4×) than those in western Tibet (3.2–8.6×) (Hudson and Quade, 2013). Because eastern and western Tibet each present regionally coherent pictures of lake expansions during the early Holocene, we can assess model reliability by comparing simulated early Holocene precipitation estimates between non-glaciated basins within eastern and western Tibet. To be consistent with their smaller expansions, lakes in the eastern Tibetan Plateau must have experienced early Holocene basin precipitation increases less than the 55% above modern modeled for Baqan Tso, with correspondingly lower increases in relative humidity. Quantifying paleoprecipitation across Tibet will allow for a better understanding of the long term climate asymmetry seen in the different lake area expansions between eastern and western lakes at their highstands (Hudson and Quade, 2013). Additionally, creating shoreline paleoprecipitation simulations for basins with more qualitative core-based proxy interpretations (e.g., pollen) may allow testing of the bias associated with the proxy.

## Conclusions

The Baqan Tso lake shoreline chronology shows overall similarities to other Holocene-age lake core and shoreline records from Tibet. Lake levels at Baqan Tso and nearby Ngangla Ring Tso generally decrease from the early Holocene towards the present, mirroring Northern Hemisphere summer insolation and proxy trends from other paleoclimatic archives. Several millennial-scale oscillations in lake level are superimposed on this long-term trend.

Our coupled land runoff and lake evaporation hydrologic model for Baqan Tso reproduces modern precipitation of 240 mm/yr (Kummerow et al., 1998) using modern climate inputs, indicating that the model accurately simulates basin hydrology. We estimate that an early Holocene mean annual precipitation of 380 mm/yr (140 mm/yr, or 55%, increase over today) was required to produce a lake level rise of 46 m and a 4.3 times lake area expansion compared to modern Baqan Tso. Increased

https://doi.org/10.1016/j.yqres.2014.07.011 Published online by Cambridge University Press

precipitation, not glacial meltwater flux, drove lake level changes at Baqan Tso because the basin was not glaciated during the Holocene.

We additionally developed a Holocene precipitation history of Baqan Tso basin using the modern and early Holocene lakes as end-members. Precipitation estimates are driven by the modern relative humidity vs. precipitation trend for Tibet and the assumption that this relationship is meaningful through the Holocene (i.e., Baqan Tso experienced a shift from drier modern western Tibet-like climate to wetter modern eastern Tibet-like climate during the early Holocene). Our estimated maximum errors for these precipitation estimates range from 12 to 15%. Maximum errors are calculated as the change between modeled precipitation and that required for 'wet' and 'dry' scenarios, where all climate variables are changed to require an increase or decrease in precipitation. Holocene precipitation at Baqan Tso basin generally declined towards the present and was punctuated by periods of weak precipitation associated with weak monsoon intensity visible in many other monsoon climate records in Asia (e.g. Fleitmann et al., 2003; Gupta et al., 2003; Wang et al., 2005; Cai et al., 2012). This suggests that for the Tibetan Plateau, Holocene monsoon intensity records like terrestrial pollen (e.g. Demske et al., 2009) and speleothem $\delta^{18}O$ records (e.g. Sinha et al., 2005; Cai et al., 2012) can be interpreted to record changes in monsoon rainfall amount of 55% greater than modern conditions.

## Acknowledgments

We thank David Dettman for help in the laboratory, Andrew Cohen and Jonathan Overpeck for feedback on this manuscript, and helpful critiques from anonymous reviewers. This work was supported by the Comer Science and Education Foundation as well as a Geological Society of America Graduate Student Grant to TH. We also gratefully acknowledge the financial and logistical support for fieldwork conducted during the summer of 2011 in Tibet from Dr. John W. Olsen through the Henry Luce Foundation and the American Council of Learned Societies. We thank the editor and two anonymous reviewers for helpful comments that improved this work.

## References

An, Z., Porter, S.C., Kutzbach, J.E., Wu, X., Wang, S., Liu, X., Li, X., Zhou, W., 2000. Asynchronous Holocene optimum of the East Asian monsoon. Quat. Sci. Rev. 19, 743–762. http://dx.doi.org/10.1016/S0277-3791(99)00031-1.

Benson, L.V., Paillet, F.L., 1989. The use of total lake-surface area as an indicator of climatic change: examples from the Lahontan Basin. Quat. Res. 32, 262–275.

Berger, A., Loutre, M.F., 1991. Insolation values for the climate of the last 10 million years. Quat. Sci. Rev. 10 (4), 297–317 (1991).

Bond, G., nine others, 2001. Persistent solar influence on North Atlantic climate during the Holocene. Science 294, 2130–2136.

Bookhagen, B., 2010. Appearance of extreme monsoonal rainfall events and their impact on erosion in the Himalaya. Geomagn. Nat. Hazards Risk 1, 37–50.

Brutsaert, W., 1975. On a derivable formula for long-wave radiation from clear skies. Water Resour. Res. 11 (5), 742–744. http://dx.doi.org/10.1029/WR011i005p00742.

Cai, Y., Zhang, H., Cheng, H., An, Z., Edwards, L., Wang, X., Tan, L., Liang, F., Wang, J., Kelly, M., 2012. The Holocene Indian monsoon variability over the southern Tibetan Plateau and its teleconnections. Earth Planet. Sci. Lett. 335–336 (2012), 135–144.

Christensen, J.H., Hewitson, B., Busuioc, A., Chen, A., Gao, X., Held, I., Jones, R., Kolli, R.K., Kwon, W.-T., Laprise, R., Magaña Rueda, V., Mearns, L., Menéndez, C.G., Räisänen, J., Rinke, A., Sarr, A., Whetton, P., 2007. Regional Climate Projections. In: Climate Change 2007: The Physical Science Basis. Contribution of Working Group I to the Fourth Assessment Report of the Intergovernmental Panel on Climate Change. In: Solomon, S., Qin, D., Manning, M., Chen, Z., Marquis, M., Averyt, K.B., Tignor, M., Miller, H.L. (Eds.), Cambridge University Press, Cambridge, United Kingdom and New York, NY, USA.

Conroy, J.L., Overpeck, J.T., 2011. Regionalization of present-day precipitation in the greater monsoon region of Asia. J. Clim. 24, 4073–4095. http://dx.doi.org/10.1175/2011JCLI4033.1.

Demske, D., Tarasov, P.E., Wünneman, B., Riedel, F., 2009. Late glacial and Holocene vegetation, Indian monsoon and westerly circulation in the Trans-Himalaya recorded in the lacustrine pollen sequence from Tso Kar, Ladakh, NW India. Palaeogeogr. Palaeoclimatol. Palaeoecol. 279, 172–185. http://dx.doi.org/10.1016/j.palaeo.2009.05.008.

Döberschutz, S., Frenzel, P., Haberzettl, T., Kasper, T., Wang, J., Zhu, L., Daut, G., Schwalb, A., Mäusbacher, R., 2014. Monsoonal forcing of Holocene paleoenvironmental change on the central Tibetan Plateau inferred using a sediment record from Lake Nam Co (Xizang, China). J. Paleolimnol. 51, 253–266. http://dx.doi.org/10.1007/s10933-013-9702-1.

Dykoski, C.A., Edwards, L., Cheng, H., Yuan, D., Cai, Y., Zhang, M., Lin, Y., Qing, J., An, Z., Revenaugh, J., 2005. A high-resolution, absolute-dated Holocene and deglacial Asian monsoon record from Dongge Cave, China. Quat. Sci. Lett. 233, 71–86.

Fleitman, D., Burns, S.J., Mudelsee, M., Neff, U., Kramers, J., Mangini, A., Matter, A., 2003. Holocene forcing of the Indian monsoon recorded in a stalagmite from southern Oman. Science 300, 1737–1739.

Gasse, F., Fontes, J.Ch., Van Campo, E., Wei, K., 1996. Holocene environmental changes in Baggong Co basin (western Tibet). Part 4: discussion and conclusions. Palaeogeogr. Palaeoclimatol. Palaeoecol. 120, 79–82.

Gile, L.H., Peterson, F.F., Grossman, R.B., 1966. Morphological and genetic sequences of carbonate accumulation in desert soils. Soil Sci. 101 (5), 347–360.

Gupta, A., Anderson, D.M., Overpeck, J.T., 2003. Abrupt changes in the Asian southwest monsoon during the Holocene and their links to the North Atlantic Ocean. Nature 421, 354–357.

Gupta, A.K., Moumita, D., Anderson, D.M., 2005. Solar influence on the Indian summer monsoon during the Holocene. Geophys. Res. Lett. 32, L17703. http://dx.doi.org/10.1029/2005GL022685.

Haginoya, S., Fujii, H., Kuwagata, T., Xu, J., Ishigooka, Y., Kang, S., Zhang, Y., 2009. Air–lake interaction features found in heat and water exchanges over Nam Co on the Tibetan Plateau. Scientific Online Letters on the Atmosphere. 5, pp. 172–175. http://dx.doi.org/10.2151/sola.2009-044.

Herzschuh, U., 2006. Paleo-moisture evolution in monsoonal Central Asia during the last 50,000 years. Quat. Sci. Rev. 25, 163–178.

Herzschuh, U., Winter, K., Wünneman, B., Li, S., 2006a. A general cooling trend on the central Tibetan Plateau throughout the Holocene recorded by the Lake Zigetang pollen spectra. Quat. Int. 154–155, 113–121. http://dx.doi.org/10.1016/j.quaint.2006.02.005.

Herzschuh, U., Kürschner, H., Mischke, S., 2006b. Temperature variability and vertical vegetation belt shifts during the last ~50,000 yr in the Qilian Mountains (NE margin of the Tibetan Plateau, China).

Hicks, B.B., 1972. Some evaluations of drag and bulk transfer coefficients over water bodies of different sizes. Bound.-Layer Meteorol. 3, 201–213.

Hostletler, S.W., Bartlein, P.J., 1990. Simulation of lake evaporation with application to modeling lake level variations of Harney–Malheur Lake, Oregon. Water Resour. Res. 26 (10), 2603–2612.

Hou, J., D'Andrea, W.J., Liu, Z., 2012. The influence of 14C reservoir age on interpretation of paleolimnological records from the Tibetan Plateau. Quat. Sci. Rev. 48, 67–79.

Hudson, A.M., Quade, J., 2013. Long-term east–west asymmetry in monsoon rainfall on the Tibetan Plateau. Geology 41, 351–354. http://dx.doi.org/10.1130/G33837.1.

Hudson, A.M., Quade, J., Huth, T., Guoliang, L., Olsen, J.W., Hucai, Z., 2014. Lake-level reconstruction for 2.3–12.8 ka for the Ngangla Ring Tso closed-basin lake system, southwest Tibetan Plateau. Quat. Res 83, 66–79 (in this issue).

Idso, S.B., 1981. A set of equations for full spectrum and 8- to 14-μm and 10.5- to 12.5-μm thermal radiation from cloudless skies. Water Resour. Res. 17 (2), 295–304. http://dx.doi.org/10.1029/WR017i002p00295.

Kasper, T., Haberzettel, T., Doberschütz, S., Daut, G., Wang, J., Zhu, L., Nowaczyk, N., Mäusbacher, R., 2012. Indian Ocean Summer Monsoon (IOSM)-dynamics within the past 4 ka recorded in the sediments of Lake Nam Co, central Tibetan Plateau (China). Quat. Sci. Rev. 39, 73–85.

Kondo, J., Yamazawa, H., 1986. Bulk transfer coefficient over a snow surface. Bound.-Layer Meteorol. 34, 123–135.

Kong, P., Na, C., Fink, D., Huang, F., Ding, L., 2007. Cosmogenic $^{10}Be$ inferred lake-level changes in Sumxi Co basin, Western Tibet. J. Asian Earth Sci. 29, 698–703.

Kramer, A., Herzschuh, U., Mischke, S., Zhang, C., 2010. Holocene treeline shifts and monsoon variability in the Hengduan Mountains (southeastern Tibetan Plateau), implications from palynological investigations. Palaeogeogr. Palaeoclimatol. Palaeoecol. 286, 23–41.

Kummerow, C., Barnes, W., Kozu, T., Shiue, J., Simpson, J., 1998. The Tropical Rainfall Measuring Mission (TRMM) sensor package. J. Atmos. Ocean. Technol. 15, 809–817. http://dx.doi.org/10.1175/1500-0426(1998)015<0809:TTRMMT>2.0.CO;2.

Kutzbach, J., 1980. Estimates of past climate at Paleolake Chad, North Africa, based on a hydrological and energy-balance model. Quat. Res. 14, 210–223.

Levin, I., Kromer, B., Hammer, S., 2013. Atmospheric $\Delta^{14}CO_2$ trend in Western European background air from 2000 to 2012. Tellus B 65, 20092.

Li, Y., Morrill, C., 2010. Multiple factors causing Holocene lake-level change in monsoonal and arid central Asia as identified by model experiments. Clim. Dyn. 35, 1119–1132.

Li, B., Sumin, W., Liping, Z., Yuanfang, L., 2001. 12 ka BP lake environment on the Tibetan Plateau. Sci. China 44, 324–331 (Supp).

Li, L., Yang, S., Wang, Z., Zhu, X., Tang, H., 2010. Evidence of warming and wetting climate over the Qinghai–Tibet Plateau. Arct. Antarct. Alp. Res. 42, 449–457. http://dx.doi.org/10.1657/1938-4246-42.4.449.

Li, Q., Lu, H., Zhu, L., Wu, N., Wang, J., Lu, X., 2011. Pollen-inferred climate changes and vertical shifts of alpine vegetation belts on the northern slope of the Nyainqentanglha Mountains (central Tibetan Plateau) since 8.4 kyr BP. The Holocene 21, 939–950.

Lu, X., Zhu, L., Nishimura, M., Morita, M., Watanabe, T., Nakamura, T., Wang, Y., 2011. A high-resolution environmental change record since 19 cal ka BP in Pumoyum Co, southern Tibet. Geol. 56, 2931–2940.

McCabe, G.J., Markstrom, S.L., 2007. A monthly water-balance model driven by a graphical user interface. U.S. Geological Survey Open-File report 2007-1088, (6 pp.).

Mischke, S., Kramer, M., Zhang, C., Shang, H., Herzschuh, U., Erzinger, J., 2008. Reduced early Holocene moisture availability in the Bayan Har Mountains, northeastern Tibetan Plateau, inferred from a multi-proxy lake record. Palaeogeogr. Palaeoclimatol. Palaeoecol. 267, 59–76.

Mischke, S., Weynell, M., Zhang, C., Wiechert, U., 2013. Spatial variability of $^{14}C$ reservoir effects in Tibetan Plateau lakes. Quat. Int. 313-314, 147–155.

Morrill, C., 2004. The influence of Asian summer monsoon variability on the water balance of a Tibetan Lake. J. Paleolimnol. 32, 273–286.
Morrill, C., Overpeck, J.T., Cole, J.E., Liu, Kam-bui, Shen, C., Tang, L., 2006. Holocene variations in the Asian Monsoon inferred from the geochemistry of lake sediments in central Tibet. Quat. Res. 65, 232–243.
Mügler, I., Gleixner, G., Gunther, F., Mäusbacher, R., Daut, G., Schütt, B., Berking, J., Schwalb, A., Schwark, L., Xu, B., Yao, T., Zhu, L., Yi, C., 2010. A multi-proxy approach to reconstruct hydrological changes and Holocene climate development of Nam Co, central Tibet. J. Paleolimnol. 43, 625–648.
Overpeck, J., Anderson, D., Trumbore, S., Prll, W., 1996. The southwest Indian Monsoon over the last 18000 years. Clim. Dyn. 12, 213–225.
Owen, L.A., 2009. Latest Pleistocene and Holocene glacier fluctuations in the Himalaya and Tibet. Quat. Sci. Rev. 28, 2150–2164. http://dx.doi.org/10.1016/j.quascirev.2008.10.020.
Reimer, P., Baillie, L., Bard, E., Bayliss, A., Beck, W., Blackwell, G., Bronk Ramsey, C., Buck, E., Burr, S., Edwards, L., Friedrich, M., Grootes, M., Guilderson, P., Hajdas, I., Heaton, J., Hogg, G., Hughen, A., Kaiser, F., Kromer, B., McCormac, G., Manning, W., Reimer, W., Richards, A., Southon, R., Talamo, S., Turney, M., van der Plicht, J., Weyhenmeyer, E., 2009. IntCal09 and Marine 09 radiocarbon age calibration curves, 0–50,000 years kcal BP. Radiocarbon 51, 1111–1150.
Rupper, S., Roe, G., Gillespie, A., 2009. Spatial patterns of Holocene glacier advance and retreat in Central Asia. Quat. Res. 72, 337–346.
Seong, B.Y., Owen, L.A., Yi, C., Finkel, R.C., 2009. Quaternary glaciation of Muztag Ata and Kongur Shan: evidence for glacier response to rapid climate changes throughout the Late Glacial and Holocene in westernmost Tibet. GSA Bull. 121 (3/4), 348–365. http://dx.doi.org/10.1130/B26339.1 (March/April 2009).
Shen, J., Liu, X., Wang, S., Ryo, M., 2005. Palaeoclimatic changes in the Qinghai Lake area during the last 18,000 years. Quat. Int. 136, 131–140.
Sinha, A., Cannariato, K.G., Stott, L.D., Li, H.C., You, C.F., Cheng, H., Edwards, R.L., Singh, I.B., 2005. Variability of Southwest Indian summer monsoon precipitation during the Bølling–Ållerød. Geology 33, 813–816.
Stuiver, M., Reimer, R.W., 1993. Extended 14C database and revised CALIB radiocarbon calibration program. Radiocarbon 35, 215–230.
Styron, R.H., Taylor, M.H., Sundell, K.E., Stockli, D.F., Oalmann, J.A.G., McAllister, A.T., Liu, D., Ding, L., 2013. Miocene initiation and acceleration of extension in the South Lunggar rift, western Tibet: evolution of an active detachment system from structural mapping and (U–Th)/He thermochronology. Tectonics 32. http://dx.doi.org/10.1002/tect.20053.
Thornthwaite, C.W., 1948. An approach toward a rational classification of climate. Geogr. Rev. 38, 55–94.
Tian, L., Yao, T., MacClune, K., White, J.W.C., Schilla, A., Vaughn, B., Vachon, R., Ichiyanagi, K., 2007. Stable isotopic variations in west China: a consideration of moisture sources. J. Geophys. Res. 112, D10112. http://dx.doi.org/10.1029/2006JD007718.
Van Campo, E., Gasse, F., 1993. Pollen- and diatom-inferred climatic and hydrological changes in Sumxi Co Basin (western Tibet) since 13,000 yr B.P. Quat. Res. 39, 300–313.
Wang, Y., Cheng, H., Edwards, R.L., Kong, X., An, Z., Wu, J., Kelly, M.J., Dykoski, C.A., Li, X., 2005. The Holocene Asian Monsoon: links to solar changes and North Atlantic climate. Science 308, 854–857.
Wang, Y., Cheng, H., Edwards, R.L., Kong, X., Shao, X., Chen, S., Wu, J., Jiang, X., Wang, X., An, Z., 2008. Millennial- and orbital-scale changes in the East Asian monsoon over the past 224,000 years. Nature 451, 1090–1093. http://dx.doi.org/10.1038/nature06692.
Wischnewski, J., Mischke, S., Wang, Y., Herzschuh, U., 2011. Reconstructing climate variability on the northeastern Tibetan Plateau since the last Lateglacial—a multi-proxy, dual-site approach comparing terrestrial and aquatic signals. Quat. Sci. Rev. 30, 82–97.
Wolock, D.M., McCabe, G.J., 1999. Explaining spatial variability in mean annual runoff in the conterminous United States. Clim. Res. 11, 149–159.
Wunneman, B., Demske, D., Tarasov, P., Kotlia, B.S., Reinhardt, C., Blowmendal, J., Diekmann, D., Hartmann, K., Krois, J., Riedel, F., Arya, N., 2010. Hydrological evolution during the last 15 kyr in the Tso Kar lake basin (Ladakh, India), derived from geomorphological, sedimentological and palynological records. Quat. Sci. Rev. 29, 1138–1155.
Yi, C., Chen, H., Yang, J., Liu, B., Fu, P., Liu, K., Li, S., 2008. Review of Holocene glacial chronologies based on radiocarbon dating in Tibet and its surrounding mountains. J. Quat. Sci. (ISSN: 0267-8179) 23, 533–543.

https://doi.org/10.1016/j.yqres.2014.07.011 Published online by Cambridge University Press